[American Journal of Science, Vol. 314, December, 2014, P. 1462–1512, DOI 10.2475/10.2014.03]

GEOMORPHIC PROCESS RATES IN THE CENTRAL ATACAMA DESERT, CHILE: INSIGHTS FROM COSMOGENIC NUCLIDES AND IMPLICATIONS FOR THE ONSET OF HYPERARIDITY

CHRISTA PLACZEK*, DARRYL E. GRANGER**, ARI MATMON***, JAY QUADE§, and URI RYB§§

ABSTRACT. Water plays a critical role in erosion and sediment transport and this relationship is most evident in the hyperarid Atacama Desert of Northern Chile, a region characterized by erosion rates that fall to near zero and cobbles and boulders with cosmogenic nuclide concentrations indicative of exposure for many millions of years. Cosmogenic nuclide concentrations from the Atacama are used to both determine the age of hyperaridity onset and to place important constraints on rates of geomorphic processes in this uniquely arid environment. Prior determinations of cosmogenic nuclide concentrations from the Atacama Desert focus primarily on exposure ages from boulders/cobbles or erosion rates from bedrock. However, recent determinations of cosmogenic nuclide concentrations from boulders, bedrock, and sediment at the same location suggests that material from diverse sample types have different cosmogenic nuclide concentrations. Therefore, it is critical to determine which concentrations of cosmogenic nuclides are most representative of overall erosion rates from the Atacama.

Here, concentrations of cosmogenic nuclides in more than 100 samples across two east-west transects within the central Atacama Desert (22-26°S) of Northern Chile are considered. Concentrations of ^{10}Be and ^{26}Al were measured in samples of bedrock, alluvial sediment, active stream sediment, and boulders within several sub-regions of the Atacama Desert, including: the western and eastern Coastal Cordillera, the inner absolute desert (including the Cerro de los Tetas), the Cordillera Domeyko, and the western flank of the Andes. This data allows detailed comparisons of cosmogenic nuclides concentrations both within diverse sample types at a given site and between major geomorphic sub-regions of the Atacama. The general pattern of cosmogenic nuclide concentrations in hyperarid environments is characterized by concentrations that are higher in boulders, moderately high in bedrock, lower in hillslope sediment, and lowest in channels that flow across the desert. At many locations in the central Atacama, boulders and bedrock have erosion rates as much as an order of magnitude slower than that of finer grained sediment at the same location, a relationship that is attributed to the fact that boulders sit above thick gypcrete soils. The hillslope to basin concentrations of cosmogenic nuclides within each sub-region, along with ^{26}Al/^{10}Be ratios, suggests that concentrations of ^{10}Be in most bedrock and sediments reflects erosion rates. However, in the western Coastal Cordillera ^{10}Be concentrations in sediment also reflects transport time.

The overarching trend in this data set is that inferred erosion rates are lower to both the east and the west, corresponding with increases in both precipitation and erosion rates towards both the Andean Flank and in the Coastal Cordillera. This trend is previously noted for the Atacama; however, this large data set allows the first observation of the influence of other variables upon erosion rates. Most notably, another clear influence on erosion rates in the Atacama is slope. In some cases, differences in slope are enough to overcome the influence of aridity. For example, erosion rates on the flanks of the Cordillera Domeyko are faster (>1 m/Ma) than that

* Centre for Tropical Environmental and Sustainability Science (TESS) & School of Earth and Environmental Sciences, James Cook University, Townsville, QLD4811, Australia; christa.placzek@jcu.edu.au
** Purdue Rare Isotope Measurement (PRIME) lab, Purdue University, West Lafayette, Indiana 47907, USA
*** Ari Matmon, Institute of Earth Sciences, Hebrew University, Jerusalem, 91904, Israel
§ Department of Geosciences, University of Arizona, Tucson, Arizona, 85721, USA
§§ Institute of Earth Sciences, Hebrew University, Jerusalem, 91904, Israel

at the crest (<0.5 m/Ma), despite the fact that the crest of this mountain range receives more moisture. Moreover, erosion rates in boulders are up to an order of magnitude slower than that of finer grained sediment. Taken together, these patterns suggest that in the extreme environment of the central Atacama erosion rates are sensitive not only to direct changes in precipitation but also to variables such as slope and soil cover. The relationship between decreased erosion and either low slope or subaerial exposure in the Atacama is potentially stronger than similar relationships documented elsewhere. These results are part of a growing body of research suggesting that even in extreme environments erosion is a complex process controlled by a multitude of variables, and where erosion rates are strongly limited by one variable, any other variable that acts to increase erosion may also have a significant effect. These new insights invoke reexamination of the global relationship between erosion and precipitation, and it is suggested that precipitation has an increasingly greater impact on erosion rates at lower values, but with some influence beginning at rates of ~1000 mm/year.

Understanding process rates in the central Atacama is essential to interpretation of cosmogenic nuclide concentrations as the timing of the onset of hyperaridity. Previous cosmogenic nuclide studies in the Atacama have specifically targeted remnant boulders to determine the age of initial aridification and this new data set shows that the boulders do not have the same cosmogenic nuclide concentration as the sediment on which they rest. Thus, the use of boulder ages or hillslope ages for the purpose of topographic reconstruction can be problematic despite the fact that, broadly, exposure of boulders and cobbles over million-year timescales implies lack of erosion over this same period. Several aspects of these results suggest that the onset of hyperaridity in the Atacama Desert predates the Pliocene. First, a number of ages from boulders predate the Pliocene. Second, new Miocene age constraints from a surface previously identified as Pliocene was shown; the age of this surface previously formed a critical component in arguments for decreased incision rates in the late Pliocene. Third, it is shown that a site that is today very sensitive to sediment fluxes from modern storm events is at least 3 Ma in age. Finally, it is shown that most of the hillslopes in the central Atacama were exposed during the Quaternary and do not have complex exposure history; this indicates that the Atacama is not and probably never has been a frozen or static landscape.

Key words: Atacama, erosion, cosmogenic nuclides, climate, precipitation

INTRODUCTION

Water is widely recognized as a key driver of erosion (for example, Langbein and Schumm, 1958,) first by promoting weathering, and second through transport of generated sediment. However, many cosmogenic nuclide-based studies suggest that climate has only a secondary role in regulating erosion rates (for example, von Blanckenburg, 2006; Portenga and Bierman, 2011; Willenbring and others, 2013). The Atacama (fig. 1) is one of the driest places on Earth and yields rocks with very high cosmogenic nuclide concentrations (Nishiizumi and others, 2005; Dunai and others, 2005; Kober and others, 2007; Evenstar and others, 2009; Placzek and others, 2010; Owen and others, 2011; Amundson and others, 2012; Owen and others, 2013). These exceptionally high cosmogenic nuclide concentrations are considered critical evidence for the antiquity of the Atacama Desert (Nishiizumi and others, 2005; Dunai and others, 2005; Evenstar and others, 2009; Amundson and others, 2012) and also imply that erosion rates in the Atacama Desert are near zero (Nishiizumi and others, 2005; Kober and others, 2007; Kober and others, 2009; Placzek and others, 2010; Owen and others, 2011). Recent cosmogenic nuclide-based studies suggest that erosion (Placzek and others, 2010), soil formation (Owen and others, 2011), and fluvial activity (Jungers and others, 2013) are ongoing, but slow in the central Atacama. Prior determinations of cosmogenic nuclide concentrations from the Atacama Desert focus primarily on results from boulders/cobbles (Nishiizumi and others, 2005; Dunai and others, 2005; Evenstar and others, 2009; Amundson and others, 2012) or bedrock (Kober and

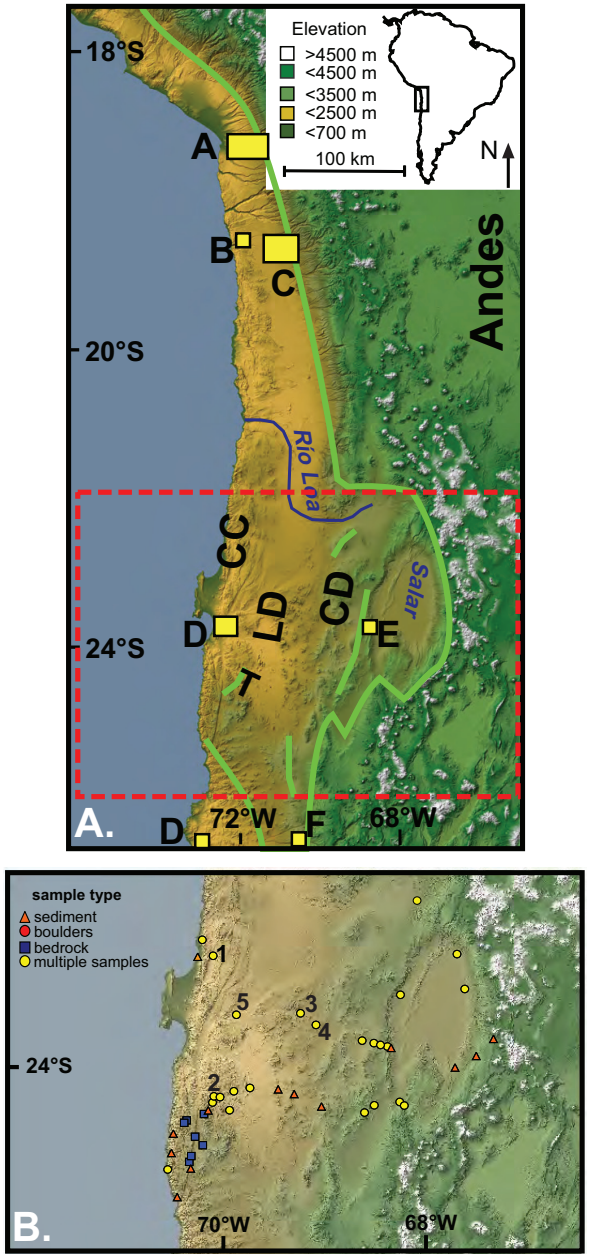

Fig. 1. (A) Location of the Atacama Desert. Sites of previous cosmogenic nuclide studies are shown with boxes. A is Kober and others, 2007; B is Dunai and others, 2005; C is Evenstar and others, 2009; D is Owen and others, 2011, 2013, and Jungers and others, 2013; D is Davis and others, 2014; F is Nishiizumi and others, 2005. The approximate location of transects in this study are denoted by the red dashed line. The Coastal Cordillera (C.C.), longitudinal depression (L.D.), Cordillera Domeyko (C.D.) and Cerro de los Tetas (T) are shown. The bright green line represents the limit of perennial vegetation. (B) Location of samples described in text. Samples of sediment are represented by orange triangles, boulders by red circles, bedrock by blue squares, and sample sites with multiple samples are represented by yellow circles. Sites described in detail are numbered one through five.

others, 2007; Owen and others, 2011), with concentrations from boulders/cobbles generally interpreted as exposure ages (Nishiizumi and others, 2005; Dunai and others, 2005; Evenstar and others, 2009; Amundson and others, 2012) and cosmogenic nuclide concentrations from bedrock (Kober and others, 2007; Placzek and others, 2010; Owen and others, 2011) interpreted as erosion rates.

Further understanding of where and at what rates erosion occurs in the Atacama is essential to understanding the relationship between slow erosion and hyperaridity. Prior determinations of erosion rates from the central Atacama focused primarily on bedrock and are hindered by possible complex exposure histories indicated by low $^{26}Al/^{10}Be$ ratios (Owen and others, 2011). Moreover, recent determinations of cosmogenic nuclide concentrations from boulders, bedrock, and sediment at the same location suggests that material from diverse sample types may have different cosmogenic nuclide concentrations and suggests that the concentration of cosmogenic nuclides from sediment may be most representative of overall erosion rates (Placzek and others, 2010). Globally, environmental variables other than precipitation impact erosion rates to a much greater degree than precipitation (for example, von Blanckenburg and others, 2006; Portenga and Bierman, 2011; Willenbring and others, 2013), with correlations between erosion rates and slope and tectonic uplift being the best documented. For example, a strong relationship between erosion rate and tectonic uplift is suggested by several previous studies in diverse environments (Riebe and others, 2001a, 2001b, 2003). The relationship between slope and erosion rate is pronounced globally (for example, Ahnert, 1970; Portenga and Bierman, 2011; Willenbring and others, 2013; fig. 2B) and slope and erosion rate are strongly correlated in the western Andes between 27° and 40°S (Carretier and others, 2013). However, no prior studies within the Atacama examine erosion rates over a variety of slopes. To fully understand the relationship between climate and landscape evolution in the Atacama, it is, therefore, necessary to evaluate not only the direct effect of aridity, but also how this aridity interacts with other critical environmental variables, such as slope and soil cover. To do so requires a detailed examination of cosmogenic nuclide concentrations in various types of samples (outcrops, sediments, and boulders) over a range of climatic and geologic settings within the Atacama.

The climatic history of the Atacama Desert between the Miocene and the Quaternary remains unresolved. Many argue for a Miocene or earlier onset of hyperaridity in the Atacama (Alpers and Brimhall, 1988; Hoke and others, 2004; Niishiizumi and others, 2005; Dunai and others, 2005; Arancibia and others, 2006; Rech and others, 2006; Davis and others, 2014; Jordan and others, 2014). While others argue for a Pliocene to Pleistocene onset of hyperaridity (Hartley and Chong, 2002; Amundson and others, 2012; Jungers and others, 2013). Other studies suggest a complex history of aridification that is punctuated by wetter events (Evenstar and others, 2009; Lehmann, ms, 2013; Jordan and others, 2014). Cosmogenic nuclide concentrations in rocks from the Atacama are considered either evidence for the antiquity (Nishiizumi and others, 2005; Dunai and others, 2005; Evenstar and others, 2009) or relative youth (Amundson and others, 2012; Jungers and others, 2013) of the Atacama Desert. These diverse interpretations are, in part, a result of different sampling strategies (that is, boulders versus sediments; stable versus unstable cosmogenic nuclides), but underscore the need for determining the cosmogenic nuclide concentration from a variety of landscape features in the region in order to shed light on the Late Miocene to Quaternary climate history of the Atacama.

Here, cosmogenic nuclide concentrations of outcrops, sediments, and boulders are examined in all sub-regions of the Atacama Desert: the western and eastern Coastal Cordillera, the inner absolute desert (including the Cerro de los Tetas), the Cordillera Domeyko, and the western flank of the Andes (fig. 1). The concentrations of ^{10}Be and

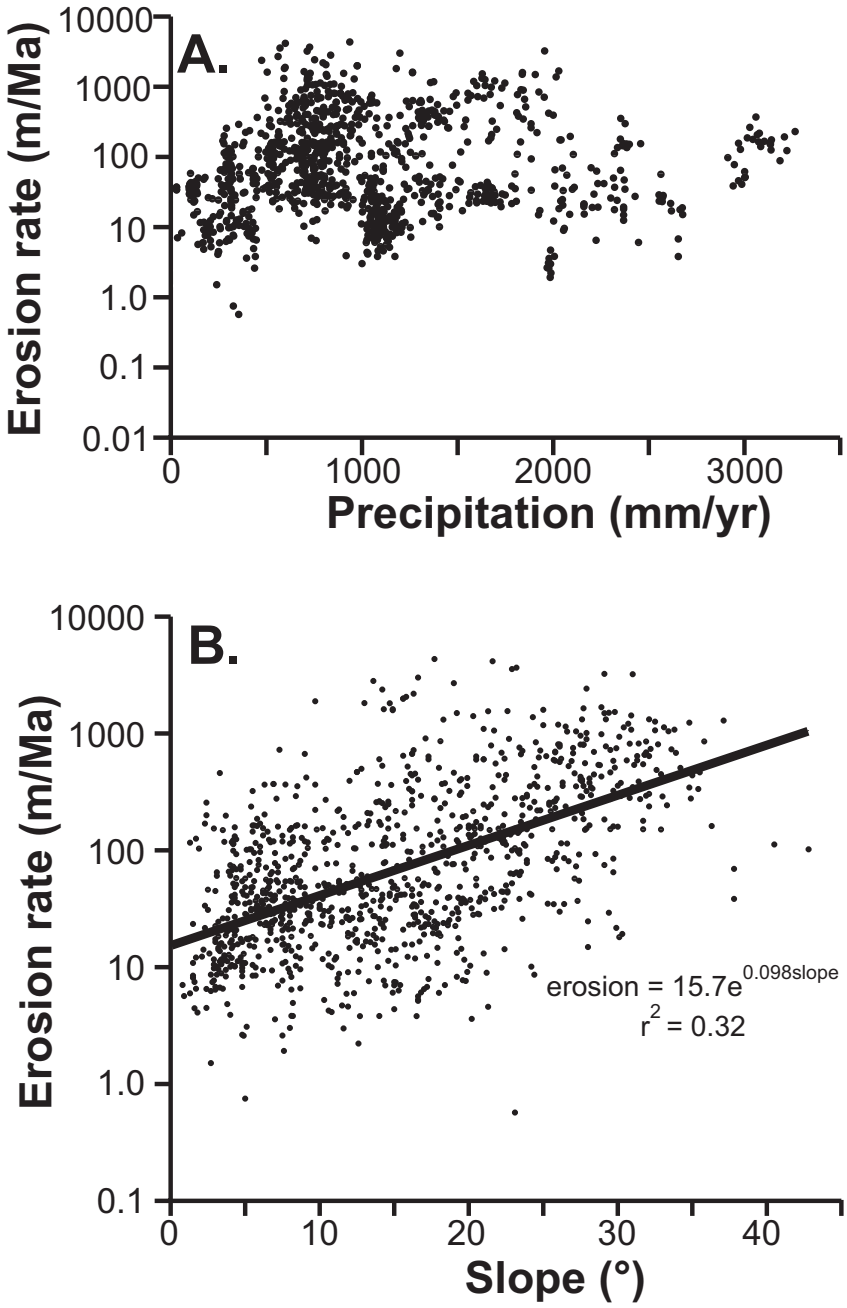

Fig. 2. (A) Erosion verses precipitation over the range of zero to 3500 mm/yr and 0 to 1000 mm/yr. Data from Portenga and Bierman (2011). (B) Erosion rate verses slope in the same data set as above.

^{26}Al were measured in over 100 samples along two east-west transects across the central Atacama Desert (fig. 1B). Within these transects are smaller hillslope to basin transects and these hillslope to basin measurements of cosmogenic nuclides allows accurate

interpretation of cosmogenic nuclide concentrations. This large data set allows comparisons both between major geomorphic sub-regions of the Atacama and within various landscape elements at sites representative of each sub-region. This allows determination of the influences of slope, uplift rate, and soil cover on erosion rates across the region. Understanding these processes in the central Atacama is essential to interpretation of cosmogenic nuclide concentrations and the timing of the onset of hyperaridity.

STUDY AREA

The Atacama Desert of northern Chile and southern Peru is located between the central Andes and the Pacific Ocean (fig. 1) at 22°S to 26°S latitude. The entire region is located in the tectonically active Andean forearc (Clift and Hartley, 2007) and has four major morphotectonic divisions. From west to east these divisions are: the Coastal Cordillera; the Central Depression; the Cordillera Domeyko; and the Western Andean Flank (fig. 1A). Many subduction trench-parallel extensional features are observed both offshore and in the Coastal Cordillera (Clift and Hartley, 2007), where recent uplift is documented by raised marine terraces (Ortlieb and others, 1996). A prominent coastal escarpment separates the narrow coastal plain from the ~1500 m high Coastal Cordillera, which locally contains peaks up to 3000 meters. Significant uplift of the entire region is suggested during the last 2 Ma (Ortlieb and others, 1996; Clift and Hartley, 2007). The Atacama fault system bounds the eastern slopes of the Coastal Cordillera with either extensional (Gonzalez and others, 2003) or strike-slip (Scheuber and Andriessen, 1990) motion. This fault system divides the Coastal Cordillera from the Central Depression, a major north-south trending intermountain region between the Coastal Cordillera and the Cordillera Domeyko. The Central Depression is filled with thick sediments including many volcanic ashes (Placzek and others 2009b) and hillslopes are overlain by widespread saline soils (Ewing and others, 2006; Rech and others 2006). Within the Central Depression, small mountains such as the Cerro de los Tetas reach elevations up to 3000 m (fig. 1). Extensive bajadas and pediments are found on both sides of the Cordillera Domeyko, and faulting and tilting of these older deposits indicates compressional deformation (Audin and others 2003; Pananont and others, 2004; Jordan and others, 2010). Internally drained basins, such as the Salar de Atacama and Salar de Punta Negra, are located east of the Cordillera Domeyko at the foot of the Andean highland. The volcanic peaks in the western Cordillera of the Andes reach elevations over 6000 meters (fig. 1A).

CLIMATE

Modern Climate

The extreme aridity of the Atacama results from several factors that exclude both Atlantic and Pacific moisture from its dry interior. These include the Andean rainshadow, the Humboldt Current, and a latitudinal position in descending air of Hadley circulation (Houston and Hartley, 2003). Precipitation stations in the region are scarce. Much of the core area of the Atacama is too dry to support vegetation and, here, the term "absolute desert" is used to refer to the hyperarid, plantless section of the Atacama Desert. Moisture along the fringes of the Atacama Desert has three sources: 1) the South American Summer Monsoon (SASM), which brings scant Atlantic moisture over the Andes; 2) Pacific cold fronts, and 3) Pacific cut-off low pressure systems. The geographic variability in the boundary of the absolute desert is directly linked to the relative importance of these precipitation sources (fig. 3).

The SASM, which originates from moisture to the northeast, principally impacts the eastern margin of the Atacama during the austral summer. Along the Andean margin of the Atacama, summer precipitation associated with the SASM spills over the

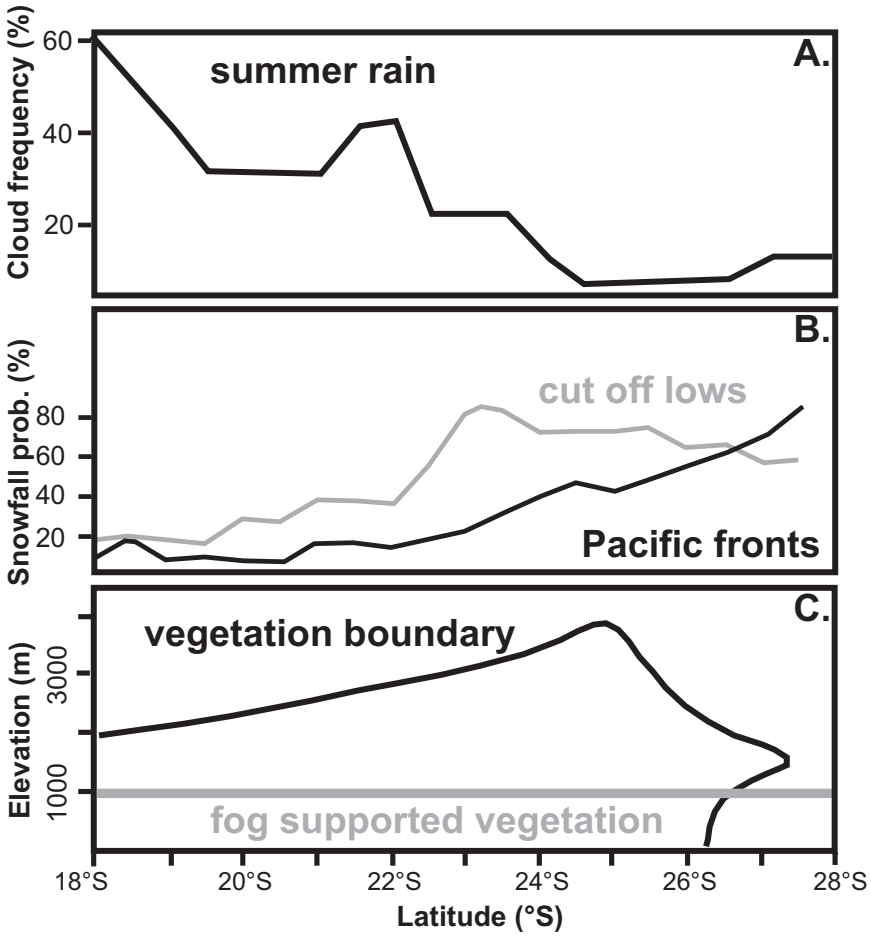

Fig. 3. Rainfall in the central Atacama has three sources, the South American summer monsoon, Pacific fronts, and cutoff-lows that migrate north from the Southern Westerlies. (A) The percent summer convective cloud cover reflects the relative intensity of precipitation originating from the South American summer monsoon (Ammann and others, 2001). This system mostly affects the northern part of the Atacama Desert. (B) The relative probability of snowfall from Pacific fronts (black line) and cutoff lows (gray lines) reflect Pacific moisture (after Vuille and Ammann, 1997). These systems mostly affect the southern part of the Atacama Desert. (C) The absolute desert is located above the fog zone (~1000 m asl) and below the reappearance of vegetation on the Andean Flank (green line in fig. 1). This boundary reaches a maximum elevation between 24 and 25°S (after Latorre and others, 2002). The elevation of the absolute desert doubles back between 26 and 27°S because of the track of Pacific fronts.

central Andes. Generally, the Andes act as an effective barrier between tropical moisture originating in the Amazon (Vuille and Keimig, 2004); however, during the summer, continental heating drives convective precipitation over the Andes (Zhou and Lau, 1998) bringing scant amounts of precipitation onto the fringes of the Atacama Desert (Ammann and others, 2001).

During the winter, the Atacama Desert experiences rainfall that originates from the Pacific. These Pacific air masses occur as either cold fronts or as polar air masses that have been cut off from the southern Westerlies (Vuille and Ammann, 1997). Pacific fronts are the main source of winter moisture in the region, as cut-off lows contribute very little to the regional water budget (Vuille and Ammann, 1997). In

addition to impacting the Coastal Cordillera every winter, Pacific air masses generate precipitation when they intercept the Andean flank, Cordillera Domeyko, and other high elevation ranges such as the Cerro de los Tetas. This Pacific moisture is the most likely source of the very rare rainfall events that occur in the absolute desert today (Vuille and Ammann, 1997). Pacific sea-surface temperature gradients modulate penetration and formation of winter precipitation events, resulting in increased rainfall in the Coastal Cordillera during El Niño years (Dillon and Rundel, 1990). The cold Pacific waters also produce a zone of heavy fog that is limited to a narrow elevation band (<1000 m) along the Coastal Cordillera.

Climate History

Hyperaridity in the Atacama requires both orographic exclusion of Atlantic moisture and exclusion of Pacific moisture by the cold Humbolt Current and to a lesser extent by the high elevation Coastal Cordillera. Changes in climate around and within the Atacama Desert occur over a variety of timescales (for example, Placzek and others, 2009a). For example, SASM intensity has experienced millennial scale variations over the Pleisotocene (for example, Betancourt and others, 2000; Rech and others, 2002; Latorre and others, 2002; Latorre and others, 2005; Placzek and others, 2013). While increased precipitation in the Andean highlands translates into higher watertables in the Atacama (Betancourt and others, 2000; Rech and others, 2002), the modern SASM does not appear to cause precipitation in the core of the absolute desert and has probably not resulted in significant rainfall since the establishment of the Andean rainshadow. Over longer timescales, multiple lines of evidence indicate hyperaridity before 10 Ma (for example, Alpers and Brimhall, 1988; Hoke and others, 2004; Niishiizumi and others, 2005; Dunai and others, 2005; Arancibia and others, 2006; Rech and others, 2006; Jordan and others, 2014), often attributed to the rise of the Andes and the formation of an orographic rainshadow. The considerable range of proposed ages for the onset of aridity in the Atacama suggest that this aridification was not unidirectional, but rather pulsed, with episodic alterations between arid and hyperarid (Evenstar and others, 2009; Lehmann, ms, 2013; Jordan and others, 2014).

Over the Oligocene and Early Miocene, the relationship between central Andean uplift and climate change in the region is a critical and unresolved question. Arguments for both the onset of Atacama aridity (for example, Hoke and others 2004) and major uplift of the high Andean plateau (the Altiplano) (for example, Garzione and others, 2006) around or after 10 Ma exist; while others invoke slower uplift (for example, Barnes and others, 2006) and an onset of aridity as early as the Oligocene (Dunai and others, 2005). One of the primary lines of evidence that is used to support both a landscape and climate that have remained stable and hyperarid over many millions of years are extremely high cosmogenic nuclide concentrations from individual cobbles or boulders. These high concentrations of cosmogenic nuclides are observed in samples from both the northern and southern reaches of the Atacama (fig. 1A) and result in surface exposure ages of 9 to 25 Ma, some of the longest exposure periods found anywhere on Earth (Niishiizumi and others, 2005; Dunai and others, 2005). A ~15 Ma age for the onset of aridity is also suggested by the termination of supergene mineralization (for example, Alpers and Brimhall, 1988; Arancibia and others, 2006), and the accumulation of nitrate soils, which are only deposited under hyperarid conditions, between 19 and 13 Ma (Rech and others, 2006). Cosmogenic nuclide concentrations in buried sediment in the Cordillera Domeyko also indicate consistent erosion rates over the last 10 Ma (Davis and others, 2014). Furthermore, changes in stream morphology indicative of a transition to dryer conditions on the Andean flank also date to ~10 Ma (Hoke and others, 2004).

Shifts in climate after 10 Ma likely post-date establishment of the Andean rainshadow and have been attributed to changes in moisture originating from the

Pacific. For example, Pliocene evaporite basins west of where salt pans occur today and the presence of Miocene fluviolacustrine and alluvial fan sediments across the Atacama suggest a transition from arid to hyperarid conditions which occurred as recently as 3 Ma (Hartley and Chong, 2002). Geomorphic evidence coupled with cosmogenic nuclide ages and K-Ar ages of ash beds in the central Atacama are interpreted to suggest whole-scale landscape stripping between the late Miocene and early Pliocene, with decreased precipitation occurring in the late Pliocene (Amundson and others, 2012). Jungers and others (2013) report that depth profiles from Quaternary sediments at a site in the central Atacama have $^{10}Be/^{21}Ne$ ratios indicative of a complex exposure history, whereas a Pliocene terrace does not have $^{10}Be/^{21}Ne$ ratios indicative of a complex exposure history. From this contrast, rapid sediment stripping is inferred under a wetter Pliocene climate (Jungers and others, 2013). In the northern Atacama, detrital zircon, K-Ar, and Ar-Ar ages, coupled with soil and sediment characterization, suggests that the last major phase of aridification is mid-Miocene in age, but with minor pulses of moisture into the Pleistocene (Lehmann, ms, 2013; Jordan and others, 2014). Pulsed development of planation surfaces in the northern Atacama is constrained between the early Miocene and the Quaternary using cosmogenic ^{3}He exposure ages of boulders (Evenstar and others, 2009). Peak development occurred in the mid-Miocene, but these surfaces continued to form into the Pleistocene (Evenstar and others, 2009).

METHODS

Sampling

Sampling efforts are focused on two transects, one along ~24°S, where the Andean rainshadow is most pronounced, and one along ~23.5°S (fig. 1). Both transects extend from the Pacific coast to the Andean foothills, including the eastern and western sides of the Coastal Cordillera, the hyperarid core of the Atacama Desert, and the Cordillera Domeyko (fig. 4). The southern transect also includes samples from the Cerro de los Tetas, an unusually high set of hills within the absolute desert. Concentrations of ^{26}Al and ^{10}Be were determined from the granitic to andesitic bedrock boulders, as well as sediment from alluvial surfaces, fluvial channels, and hillslopes (tables 1, 2, and 3); a few samples of amalgamated quartz clasts were also collected (table 1). Our sampling effort focused not only on a transect approach, but also on comparisons of multiple samples from bedrock, boulders, and sediments of different sizes at the same site and on hillslope to basin transects within each subregion.

Cosmogenic Nuclide Methods

Secondary cosmic rays interacting with rocks and sediments in the uppermost few meters of the Earth's surface produce terrestrial cosmogenic nuclides (for reviews see: Gosse and Phillips, 2001; Dunai, 2010; Granger and others, 2013). At a given location, terrestrial cosmogenic nuclide concentrations depend on the residence time of mineral grains near the surface, and reflects a balance among production, radioactive decay, and erosion. To the first order, the concentration of terrestrial cosmogenic nuclides (N_i) in a rock depends on both the erosion rate (E) and the exposure time (t) (Lal, 1991):

$$N_i(t) = \left(\frac{P_i}{\rho E \Lambda^{-1} + \lambda_i}\right)(1 - e^{-(\rho E \Lambda^{-1} + \lambda_i)t}) \quad (1)$$

where P_i is the production rate, ρ is the rock density, Λ is the effective cosmic-ray nucleon attenuation length, and λ_i is the decay constant ($\lambda_{Al\text{-}26} = 9.68 \times 10^{-7}\ a^{-1}$, and

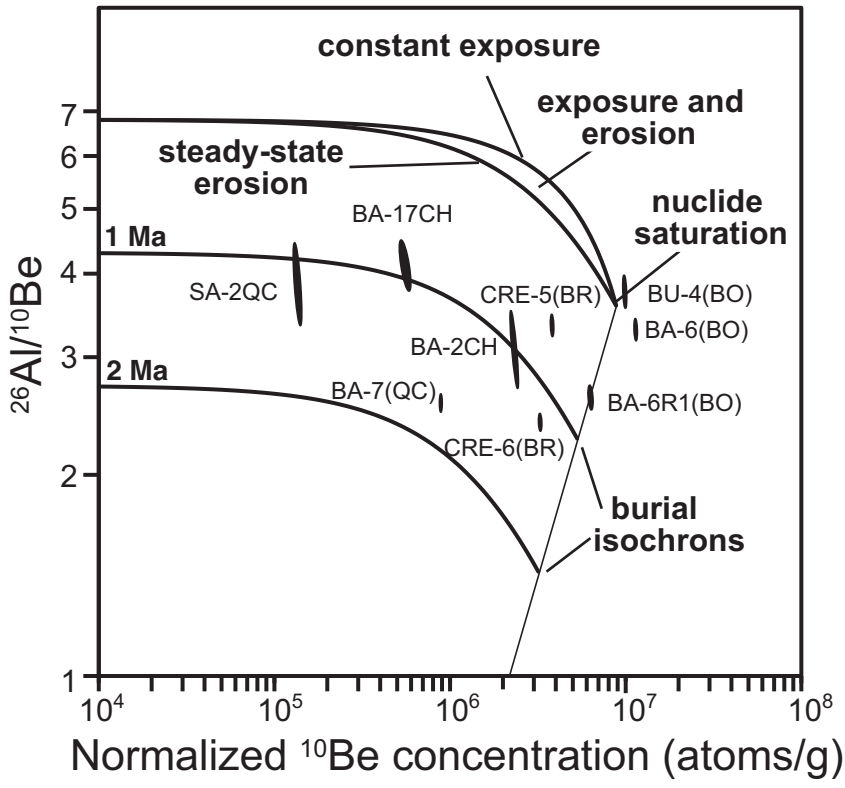

Fig. 4. Cosmogenic nuclide data for samples with a burial history or oversaturation shown on a $^{26}Al/^{10}Be$ vs. normalized ^{10}Be concentration plot. One sigma analytical errors are shown. This nuclide plot has a line indicative of constant exposure with no erosion and a line indicative of steady-state erosion. The field between these two lines represents some combination of exposure and erosion. All continuously exposed samples should fall within this space. Samples that have experienced a burial history will plot in the burial field; isochrons of 1 and 2 Ma are shown for complete burial. Abbreviations following the sample number indicate the sample type: CH is channel sediment; QC is quartz clasts; BR is bedrock, and BO is boulder. The designation for sample type is added in parentheses for the purposes of this figure where not implied by the name in table 1.

$\lambda_{Be\text{-}10} = 4.9 \times 10^{-7}$ a^{-1}; Chmeleff and others, 2010; Korschinek and others, 2010). Equation (1) assumes that the rock being analyzed has eroded at a constant rate since exposure, that it has never been buried, and that erosion rates are sufficiently slow that production by muons can be ignored (Granger and Muzikar, 2001).

As shown by Equation 1, terrestrial cosmogenic nuclide concentrations in rocks exposed at the surface are controlled by both exposure time and erosion rate. The processes by which sediments acquire cosmogenic nuclides include erosion from the bedrock, transport on hillslopes and in fluvial systems, and storage near the surface during transport and after deposition. When geomorphic context indicates that one of these processes is dominant, then cosmogenic nuclide concentrations are interpreted as either erosion rates or exposure ages. In most global settings (see for example: Lal 1991; Gosse and Phillips, 2001), the cosmogenic nuclide concentration from bedrock and sediments is interpreted as maximum erosion rates and cosmogenic nuclide concentrations from boulders are interpreted as minimum exposure ages.

If two or more cosmogenic nuclides are measured, their concentrations should be concordant with a single erosion rate and/or exposure age. If they are not, this

TABLE 1

Sample location data

Sample name	Latitude (°S)	Longitude (°W)	Elevation (m)	Sample material	Sample thickness (cm)	Precip-itation (mm/yr)
BA-10SD	-23.4037	-69.4623	1563	channel gravel	0.05	3
BA-11	-23.4034	-69.4683	1513	boulder (diorite)	3	11
BA-11#2	-23.4034	-69.4683	1513	boulder (diorite)	3	3
BA-12SDL	-23.3978	-69.4624	1527	alluvial sediment	0.5	3
BA-12SDsm	-23.3978	-69.4624	1527	alluvial sediment	0.05	3
BA-13CHL	-23.5831	-69.27688333	1857	channel gravel	0.5	3
BA-13CHsm	-23.5831	-69.2769	1857	channel gravel	0.05	3
BA-13SD	-23.5831	-69.2752	1862	alluvial sediment	0.05	3
BA-15CH	-23.6387	-68.773	2558	channel gravel	0.05	30
BA-16	-23.6519	-68.7391	2662	bedrock (diorite)	7	39
BA-17CH	-23.6912	-68.6181	2537	channel gravel	0.05	45
BA-18CH	-23.7922	-67.9736	3090	channel gravel	0.5	60
BA-22CH	-23.6118	-67.8443	3604	channel gravel	0.05	61
BA-23QC	-22.7757	-70.29065	99	quartz clasts	2	75
BA-23sm	-22.7757	-70.29065	99	channel gravel	0.05	75
BA-24sm	-22.9247	-70.2736	120	channel gravel	0.05	75
BA-25A	-22.9252	-70.1887	898	boulder (granite)	3	45
BA-25B	-22.9251	-70.1878	898	boulder (granite)	8	40
BA-25C	-22.9255	-70.1848	876	boulder (granite)	3	35
BA-25CH	-22.8951	-70.1887	960	channel gravel	0.05	50
BA-27A	-22.8959	-70.1482	969	cobble (quartz)	1	3
BA-27CH	-22.8951	-70.1482	960	channel gravel	5	15
BA-27CH	-22.8951	-70.1482	960	channel gravel	0.05	15
BA-2CH	-23.5394	-69.07963333	2472	channel gravel	0.05	7
BA-2SD	-23.5335	-69.0796	2472	alluvial sediment	0.5	7
BA-3	-23.4078	-69.4636	1740	bedrock (diorite)	8	3
BA-4	-23.4037	-69.4623	1575	boulder (diorite)	10	3
BA-4SD	-23.4037	-69.4623	1565	alluvial sediment	2	3
BA-5	-23.4001	-69.4631	1513	boulder (diorite)	10	3
BA-5SD	-23.4001	-69.4631	1517	alluvial sediment	1	3
BA-6	-23.3422	-69.9295	1009	boulder (granite)	5	1
BA-6R1	-23.3422	-69.9295	1009	boulder (granite)	3	1
BA-6R2	-23.3422	-69.9295	1009	boulder (granite)	8	1
BA-6SD	-23.3422	-69.9295	1009	alluvial sediment	0.1	1
BA-7	-23.5872	-68.8124	2479	quartz clasts	5	20
BA-8	-23.6077	-68.8156	2456	quartz clasts	5	20
BA-8A	-23.6077	-68.8156	2456	quartz clast	8	20
BA-9	-23.6715	-68.6699	2945	quartz clasts	4	43
BA-9A	-23.6715	-68.6699	2945	quartz clast	7	43
BU-4	-23.3933	-69.4704	1520	boulder (diorite)	4.5	3
CA-1CH	-22.6648	-68.4706	3196	channel gravel	0.05	50
CA-1SD	-22.6654	-68.4706	3204	alluvial sediment	4	50
CRE-1	-24.2790	-70.2993	1830	channel gravel	5	7
CRE-2	-24.2764	-70.3006	1918	bedrock (andesite)	5	7
CRE-4	-24.4342	-70.3297	2207	bedrock (andesite)	5	9
CRE-5	-24.4866	-70.3132	1944	bedrock (quartz rich vein)	5	4
CRE-6	-24.6219	-70.3716	2373	bedrock (quartz rich vein)	5	10
CRE-7	-24.6469	-70.3781	2415	bedrock (quartz rich vein)	6	11
CRE-8	-24.7089	-70.3690	2104	channel gravel	0.5	9

Table 1
(continued)

Sample name	Latitude (°S)	Longitude (°W)	Elevation (m)	Sample material	Sample thickness (cm)	Precip-itation (mm/yr)
CRW-1	-24.9121	-70.51025	216	channel gravel	0.05	40
CRW-2	-24.6601	-70.5548	148	channel gravel	1	75
CRW-3	-24.5682	-70.5411	134	channel gravel	5	75
CRW-4	-24.5261	-70.5701	24	bedrock (diorite)	5	75
CRW-5	-24.4055	-70.5294	175	channel gravel	0.05	75
CRW-7	-24.3197	-70.4800	1059	bedrock (diorite)	5	60
CRW-8	-24.31965	-70.478	1200	bedrock (granite)	8	50
CT-50	-24.2076	-70.0633	2078	bedrock (granite)	5	55
CT-51	-24.2078	-70.0633333	2078	bedrock (diorite)	3	55
CT-52	-24.2046	-70.0667	2240	bedrock (diorite)	5	55
CT-53	-24.2024	-70.0678	2184	bedrock (diorite)	5	55
CT-54	-24.2053	-70.0681	2114	bedrock (diorite)	4	55
CT-55	-24.2057	-70.06751667	2117	bedrock (diorite)	4	55
CT-56	-24.2083	-70.06821667	1979	alluvial sediment	2	52
CT-57	-24.2223	-70.06618333	1423	channel gravel	5	40
CT-58	-24.2240	-70.0648333	1374	boulder (diorite)	5	37
PC-1	-24.0693	-70.1931	1047	boulder (diorite)	7	1
PC-1A	-24.0693	-70.1931	1047	boulder (andesite)	5	1
PC-1SD	-24.06927	-70.1975	1047	alluvial sediment	0.05	1
PC-2	-24.0712	-70.1941	1070	boulder (granite)	10	1
PC-2A	-24.0712	-70.1941	1070	boulder (diorite)	20	1
PC-3	-24.0698	-70.1997	1005	boulder (andesite)	5	1
PC-3BR	-24.0698	-70.1997	1005	bedrock (diorite)	7	1
PC-4	-24.0728	-70.2037	980	quartz clast	10	1
PC-5	-24.0728	-70.2038	979	boulder (diorite)	4	1
PC-5SD	-24.0728	-70.2038	979	alluvial sediment	0.05	1
PC-6	-24.1054	-70.222	1337	bedrock (diorite)	5	1
PC-7	-24.0999	-70.2259	1222	channel gravel	3	1
S0-8BA	-24.1529	-68.547	3128	alluvial sediment	1.5	25
SA-1SD	-23.7857	-68.1071	2364	alluvial sediment	0.5	56
SA-2CC	-23.259	-68.0644	2357	quartz clasts	6	58
SA-2QC	-23.259	-68.0644	2357	quartz clast	5	58
SA-2SD	-23.259	-68.0644	2357	alluvial sediment	0.05	58
SA-3	-22.9147	-68.1193	2490	cobble (granitic)	5	55
SA-3SD	-22.9147	-68.1193	2490	alluvial sediment	0.1	55
SA-4BD	-23.2230	-68.1193	2432	boulder (andesite)	5	55
SA-4CH	-23.2232	-68.5649	2440	channel gravel	0.5	49
SO-1	-24.0932	-70.1688	1040	boulder (granite)	3	1
SO-10SD	-24.1525	-69.4278	1658	channel gravel	4	30
SO-11CH	-24.2687	-69.1975	2748	channel gravel	0.05	39
SO-12	-24.2223	-68.8961	3246	bedrock (quartz rich vein)	15	48
SO-13	-24.1978	-68.8114	3048	bedrock (quartz rich vein)	2	40
SO-13SD	-24.1955	-68.81	3028	alluvial sediment	5	40
SO-2	-24.0879	-70.1709	1165	bedrock (granite)	3	1
SO-3	-24.0887	-70.0597	1057	boulder (diorite)	3	1
SO-3R1	-24.0887	-70.0597	1057	boulder (diorite)	7	1
SO-3R2	-24.0887	-70.0597	1057	boulder (diorite)	13	1
SO-3R4	-24.0887	-70.0597	1057	boulder (diorite)	3	1
SO-3SD	-24.0887	-70.0597	1057	alluvial sediment	0.5	1

Table 1
(continued)

Sample name	Latitude (°S)	Longitude (°W)	Elevation (m)	Sample material	Sample thickness (cm)	Precip-itation (mm/yr)
SO-4	-24.03868	-69.8728	1025	boulder (diorite)	5	1
SO-4SD	-24.0384	-69.8728	1034	channel gravel	0.5	1
SO-5	-24.0092	-69.865	1438	bedrock (diorite)	5	1
SO-6	-24.1153	-68.5956	2913	boulder (granite)	3	25
SO-6SD	-24.1153	-68.5956	2913	alluvial sediment	0.5	25
SO-6WA	-24.11535	-68.5953	2916	channel gravel	1	25
SO-7	-24.1162	-68.596	2924	quartz clast	10	25
SO-8CH	-24.1529	-68.5470	3128	channel gravel	0.05	25
SO-9CH	-24.05999	-69.5324	1344	channel gravel	0.05	25
SOI-SD	-24.0933	-70.1688	1040	alluvial sediment	0.5	1

indicates that the rock has been buried. During complete or partial burial the shorter-lived nuclide decays faster than the longer-lived nuclide and the ratio between ^{10}Be and ^{26}Al can be used to estimate the burial time (see for example: Klein and others, 1986; Granger and others, 1997). For example, when production is stopped entirely in a single event the age of sediment burial and preexposure concentration can be determined because:

$$\frac{N^{26}}{N^{10}} = \left[\frac{N^{26}}{N^{10}}\right]_o e^{-t(\lambda_{26} - \lambda_{10})} \quad (2)$$

Where, $\left[\frac{N^{26}}{N^{10}}\right]_o$ is the initial ratio of ^{26}Al to ^{10}Be, $\frac{N^{26}}{N^{10}}$ is the modern ratio and t is the duration of burial (Granger and Muzikar, 2001). A more complicated scenario exists when a sample is incompletely buried or experiences multiple episodes of burial at different production rates. Multiple cosmogenic nuclides are often presented on an exposure-burial diagram, illustrating concordant erosion and exposure lines, as well as isochrons for complete burial (fig. 4); in the case of ^{26}Al/^{10}Be diagrams complete burial can be determined for burial between roughly 0.75 and 5 Ma (fig. 4). In instances where samples have not experienced burial, inferred erosion rates and/or exposure ages will be similar for both ^{26}Al and ^{10}Be concentrations. Analytical errors are generally much smaller for ^{10}Be, as such, we focus our discussion on ^{10}Be concentrations.

Several major schemes exist for normalizing terrestrial cosmogenic nuclide production rates from one location on Earth to another. In unshielded samples, the production rate of terrestrial cosmogenic nuclides varies with altitude, latitude, and time as a result of changing atmospheric depth and geomagnetic field strength. Scaling schemes differ in how these variables are taken into account (for review see Balco and others, 2008). Here, ^{10}Be and ^{26}Al concentration data from the central Atacama are presented using the more commonly applied Lal (1991)/Stone (2000) scaling scheme because it allows ready comparison to other studies. Production rates of all samples presented here are scaled to the elevation of the collection site using the CRONUS online calculator (Balco and others, 2008) and assuming no correction for uplift rate. Scaled ^{10}Be nuclide concentrations are calculated using an assumed sea

TABLE 2

Cosmogenic nuclide data

Sample name	assumed density (g cm^{-2})	Shielding correction	Be AMS standard	Al AMS standard	sample mass (g)	^{10}Be carrier (g)	$^{10}Be/^{9}Be_{measured}$ (x10^{-15})	± (x10^{-15})	$^{26}Al/^{27}Al_{measured}$	± (x10^{-15})	^{10}Be blank (x10^{-15})	^{26}Al blank (x10^{-15})	$Al/Be_{measured}^{2}$
BA-10SD	07KNSTD	KNSTD	18.8655	0.2613	3922.00	169.90	4210.00	223.20	16.827	6.05	0.26	36.51	1.94
BA-11	07KNSTD	KNSTD	5.0804	0.2576	2750	80	n/a	n/a	n/a	15.54	0.45	n/a	n/a
BA-11#2	07KNSTD	KNSTD	8.1691	0.2578	3929.00	147.20	11397.00	316.80	4.650	13.82	0.52	62.32	1.73
BA-12SDL	07KNSTD	KNSTD	3.6206	0.2552	1011.00	31.93	2100	290	7.063	7.93	0.25	38.74	5.36
BA-12SDsm	07KNSTD	KNSTD	27.6457	0.2526	10198	182	12300	400	12.298	10.40	0.19	51.47	1.68
BA-13CHL	07KNSTD	KNSTD	17.9146	0.2558	9606.00	311.30	19300	2700	6.659	15.30	0.50	68.36	9.56
BA-13CHsm	07KNSTD	KNSTD	8.2333	0.2562	4576	80	4460	280	13.079	15.88	0.28	67.48	4.25
BA-13SD	07KNSTD	KNSTD	8.8189	0.2601	6160	140	7400	400	13.025	20.26	0.46	105.79	5.73
BA-15CH	07KNSTD	KNSTD	31.2036	0.2614	17292.00	745.80	n/a	n/a	n/a	16.16	0.70	0.00	0.00
BA-16	07KNSTD	KNSTD	29.2734	0.2553	18262	316	49800	1500	6.177	17.77	0.31	99.98	3.01
BA-17CH	07KNSTD	KNSTD	11.7386	0.2595	932.90	50.30	2388.00	88.44	4.843	2.28	0.12	9.50	0.35
BA-18CH	07KNSTD	KNSTD	6.0836	0.2557	1470.00	254.90	3817.00	156.30	7.676	6.86	1.19	45.82	1.88
BA-22CH	07KNSTD	KNSTD	12.9727	0.2562	336.20	22.51	604.00	31.04	9.139	0.73	0.05	4.02	0.21
BA-23QC	07KNSTD	KNSTD	10.8019	0.2577	184.70	9.91	593.70	42.15	7.255	0.47	0.03	3.04	0.22
BA-23sm	07KNSTD	KNSTD	2.7854	0.255	44.99	6.42	477.80	119.60	1.982	0.39	0.08	3.18	0.80
BA-24sm	07KNSTD	KNSTD	7.8904	0.2577	81.62	13.25	416.70	44.36	4.654	0.27	0.05	2.32	0.25
BA-25A	07KNSTD	KNSTD	12.0582	0.2566	248	10	650	50	7.599	0.58	0.02	3.85	0.31
BA-25B	07KNSTD	KNSTD	9.0485	0.257	324	11	2610	120	2.723	1.02	0.04	7.49	0.35
BA-25C	07KNSTD	KNSTD	12.6259	0.2548	969	34	4200	400	4.294	2.18	0.08	13.53	1.29
BA-25CH	07KNSTD	KNSTD	4.6116	0.2519	416	21	1200	300	5.840	2.52	0.13	14.13	3.57
BA-27A	07KNSTD	KNSTD	8.8856	0.2549	2513	56	9600	700	3.286	8.04	0.18	33.69	2.46
BA-27CH	07KNSTD	KNSTD	6.46	0.26	1350	40	4030.00	200.00	3.974	5.98	0.18	23.69	1.18
BA-27CH	07KNSTD	KNSTD	6.4596	0.2571	1350.00	40.00	4030	200	3.974	5.98	0.18	23.69	1.18
BA-2CH	KNSTD	KNSTD	22.2593	0.2604	7830	136.9	11182	1487	5.843	10.10	0.18	28.37	3.77
BA-2SD	KNSTD	KNSTD	23.9189	0.2576	8263	249	19262	743.9	6.710	8.84	0.30	51.76	2.00
BA-3	07KNSTD	KNSTD	10.7581	0.2555	3940	120	12900	300	4.750	10.43	0.32	54.19	1.26
BA-4	07KNSTD	KNSTD	4.21	0.2608	1080	30	n/a	n/a	n/a	7.45	0.21	n/a	n/a
BA-4SD	07KNSTD	KNSTD	15.2236	0.2602	2711.00	142.70	5301.00	191.00	8.233	5.16	0.27	27.77	1.00
BA-5	07KNSTD	KNSTD	22.4462	0.2552	12000	300	10600	400	15.415	15.22	0.38	69.17	2.61
BA-5SD	KNSTD	KNSTD	12.2879	0.2583	3369	89	8984	388.5	4.455	6.92	0.21	31.20	1.36
BA-6	07KNSTD	KNSTD	41.8841	0.2578	23300.00	400.00	26100	1200	8.848	16.00	0.27	52.95	2.43
BA-6R1	07KNSTD	KNSTD	29.1341	0.2558	11084.00	320.30	15066.00	422.80	5.759	10.85	0.31	28.38	0.80
BA-6R2	07KNSTD	KNSTD	22.831	0.2545	9035.00	403.50	25218.00	1393.00	4.410	11.23	0.50	46.19	2.55

TABLE 2
(continued)

Sample name	assumed density (g cm^{-2})	Shielding correction	Be AMS standard	Al AMS standard	sample mass (g)	^{10}Be carrier (g)	$^{10}Be/^{9}Be_{measured}$ (x10^{-15})	± (x10^{-15})	$^{26}Al/^{27}Al_{measured}$	± (x10^{-15})	^{10}Be blank (x10^{-15})	^{26}Al blank (x10^{-15})	$Al/Be_{measured}$[2]
BA-6SD	07KNSTD	KNSTD	18.4368	0.2538	5270.00	238.20	13973.00	655.00	4.432	8.09	0.37	31.76	1.49
BA-7	07KNSTD	KNSTD	82.119	0.2865	8827.00	140.00	2631.00	75.40	25.979	3.43	0.05	8.88	0.25
BA-8	07KNSTD	KNSTD	19.2458	0.2549	2015.00	98.90	4301.00	104.10	15.930	2.97	0.15	33.80	0.82
BA-8A	07KNSTD	KNSTD	13.1574	0.2573	2528.00	116.40	4324.00	117.70	9.511	5.51	0.25	29.96	0.82
BA-9	07KNSTD	KNSTD	24.5121	0.2619	16290.00	799.80	22797.00	710.50	10.332	19.41	0.95	93.78	2.92
BA-9A	07KNSTD	KNSTD	66.1817	0.2549	53103.00	3224.00	51351.00	1260.00	15.073	22.82	1.39	111.11	2.73
BU-4[1]	NIST_27900	KNSTD	9.832	0.216	14090.00	98.00	37743.00	890.00	1.448	20.72	0.49	80.32	3.73
CA-1CH	07KNSTD	KNSTD	51.4416	0.2598	11457.00	726.70	n/a	n/a	n/a	6.45	0.41	0.00	0.00
CA-1SD	07KNSTD	KNSTD	25.0008	0.2604	6007.00	199.40	9944.00	392.60	11.413	6.97	0.23	44.03	1.74
CRE-1	KNSTD	KNSTD	8.943	0.2594	3632	278	14101	563.1	3.332	10.32	0.90	50.64	2.03
CRE-2	07KNSTD	KNSTD	14.6004	0.2551	4036	101	23500	1700	2.760	7.86	0.20	42.22	3.06
CRE-4	KNSTD	KNSTD	29.1792	0.2611	12754	308	38962	2763	4.769	11.38	0.31	61.90	4.39
CRE-5	07KNSTD	KNSTD	34.6373	0.2496	13344.00	194.20	18128.00	681.50	7.426	10.73	0.16	36.15	1.36
CRE-6	07KNSTD	KNSTD	20.8876	0.2557	8827.00	140.00	13389.00	390.40	4.727	12.05	0.19	28.87	0.84
CRE-7	07KNSTD	KNSTD	32.4833	0.2607	12832.00	613.00	30575.00	928.80	8.059	11.49	0.55	73.69	2.24
CRE-8	KNSTD	KNSTD	36.3183	0.2607	17534	335	63295	3028	3.592	12.58	0.27	60.79	2.91
CRW-1	07KNSTD	KNSTD	10.1832	0.2589	22.95	10.23	n/a	n/a	n/a	0.05	0.02	0.00	0.00
CRW-2	07KNSTD	KNSTD	13.3269	0.255	35.62	3.47	229.00	49.05	2.677	0.06	0.01	0.42	0.09
CRW-3	KNSTD	KNSTD	13.0967	0.2563	254	31	291.4	62.81	5.944	0.32	0.08	1.06	0.28
CRW-4	KNSTD	KNSTD	29.9868	0.2603	678	35	1851	94.41	4.769	0.51	0.04	2.78	0.15
CRW-5	07KNSTD	KNSTD	32.171	0.2569	46.74	5.48	167.40	107.70	7.622	0.04	0.01	0.36	0.23
CRW-7	KNSTD	KNSTD	10.56	0.258	873	63	3074	203.7	4.481	1.92	0.18	12.35	0.83
CRW-8	07KNSTD	KNSTD	16.6668	0.2572	1481.00	50.33	4754.00	179.90	6.022	2.54	0.09	16.44	0.62
CT-50	07KNSTD	KNSTD	14.9524	0.2583	5559.00	106.50	25987.00	473.00	3.598	10.71	0.21	60.20	1.10
CT-51	07KNSTD	KNSTD	26.4269	0.2576	11907.00	313.20	28900	2200	8.764	12.95	0.34	91.99	7.00
CT-52	07KNSTD	KNSTD	20.2816	0.2531	6455.00	235.60	18343.00	498.10	5.939	8.98	0.33	50.67	1.38
CT-53	07KNSTD	KNSTD	22.7722	0.2542	10199.00	433.70	27117.00	1256.00	6.822	12.70	0.54	76.95	3.56
CT-54	07KNSTD	KNSTD	22.2049	0.2602	7548.00	301.20	19694.00	680.50	7.167	9.86	0.39	61.63	2.13
CT-55	07KNSTD	KNSTD	29.887	0.2543	6705.00	244.70	18300	2100	9.386	6.36	0.23	54.44	6.25
CT-56	KNSTD	KNSTD	13.9025	0.2557	4395	221.8	17809	961.5	3.840	8.84	0.45	46.76	2.52
CT-57	KNSTD	KNSTD	14.4729	0.2556	3197	253.8	8002	580.4	5.918	6.12	0.49	30.99	2.25
CT-58	07KNSTD	KNSTD	18.7644	0.2554	3522.00	141.10	11300	1700	5.950	5.35	0.21	34.07	5.13
PC-1	07KNSTD	KNSTD	15.5488	0.2603	4285.00	194.00	5809.00	143.50	11.444	7.99	0.36	41.43	1.02

Table 2
(continued)

Sample name	assumed density (g cm^{-2})	Shielding correction	Be AMS standard	Al AMS standard	sample mass (g)	^{10}Be carrier (g)	$^{10}Be/^{9}Be_{measured}$ (x10^{-15})	± (x10^{-15})	$^{26}Al/^{27}Al_{measured}$	± (x10^{-15})	^{10}Be blank (x10^{-15})	^{26}Al blank (x10^{-15})	$Al/Be_{measured}^{2}$
PC-1A	07KNSTD	KNSTD	5.2041	0.2546	1146	51	4700	250	3.796	6.24	0.28	32.45	1.73
PC-1SD	07KNSTD	KNSTD	41.4096	0.2579	6150.00	148.60	11601.00	293.40	10.663	4.27	0.10	28.70	0.73
PC-2	07KNSTD	KNSTD	33.552	0.2597	4923.00	264.10	17778.00	521.60	4.717	4.25	0.23	24.19	0.71
PC-2A	07KNSTD	KNSTD	6.8621	0.2574	776.90	30.13	4722.00	454.10	3.749	3.22	0.13	24.71	2.38
PC-3	KNSTD	KNSTD	5.7569	0.2581	2519	70	7174	1410	2.750	10.94	0.36	32.76	6.48
PC-3BR	07KNSTD	KNSTD	3.8083	0.2555	755.30	25.17	2561.00	183.20	6.076	5.60	0.19	38.81	2.78
PC-4	07KNSTD	KNSTD	81.672	0.2572	22149.00	392.70	47683.00	805.00	6.606	7.78	0.14	36.97	0.62
PC-5	07KNSTD	KNSTD	15.8513	0.2584	4183.00	176.80	n/a	n/a	n/a	7.60	0.32	0.00	0.00
PC-5SD	07KNSTD	KNSTD	37.0539	0.2539	8654.00	223.60	13158.00	594.70	8.495	6.61	0.17	28.53	1.29
PC-6	07KNSTD	KNSTD	13.9183	0.2576	2417.00	117.50	8145.00	288.30	6.135	4.98	0.24	34.44	1.22
PC-7	07KNSTD	KNSTD	34.8002	0.2587	6673.00	224.80	4088.00	117.00	27.471	5.53	0.19	31.06	0.89
S0-8BA	07KNSTD	KNSTD	39.4014	0.255	8995.00	344.40	9926.00	631.60	15.978	6.49	0.25	38.23	2.43
SA-1SD	KNSTD	KNSTD	2.1266	0.2586	749	38	2508	535.3	3.347	8.04	0.58	37.34	8.12
SA-2CC	07KNSTD	KNSTD	25.26	0.2553	419.00	16.42	585.00	79.44	8.328	0.46	0.02	1.81	0.25
SA-2QC	07KNSTD	KNSTD	11.2352	0.2558	127.10	7.49	676.40	121.80	3.692	0.31	0.02	2.10	0.38
SA-2SD	07KNSTD	KNSTD	22.038	0.2562	961.00	33.41	2768.00	164.00	7.464	1.24	0.04	8.93	0.53
SA-3	KNSTD	KNSTD	55.8113	0.2572	718	37	4229	229.7	2.983	0.29	0.02	2.14	0.12
SA-3SD	07KNSTD	KNSTD	46.4878	0.2568	1833.00	80.38	1681.00	76.43	20.689	1.13	0.05	7.13	0.32
SA-4BD	KNSTD	KNSTD	3.2793	0.2576	459	104	850	80.95	3.418	2.91	0.92	8.04	0.83
SA-4CH	KNSTD	KNSTD	5.7252	0.2524	998	71	3030	409.4	4.118	4.02	0.36	20.19	2.77
SO-1	07KNSTD	KNSTD	5.8956	0.2584	1992.00	76.12	4746.00	243.50	6.174	9.71	0.37	47.80	2.45
SO-10SD	07KNSTD	KNSTD	26.5467	0.2623	6365.00	220.80	15598.00	594.00	6.338	7.01	0.24	36.40	1.39
SO-11CH	07KNSTD	KNSTD	16.293	0.2588	15128.00	540.50	n/a	n/a	n/a	26.80	0.96	0.00	0.00
SO-12	07KNSTD	KNSTD	22.4722	0.2572	16798	299	6750	190	33.961	21.45	0.38	97.62	2.76
SO-13	07KNSTD	KNSTD	28.1354	0.2528	22008	902	72700	1800	6.531	22.06	0.90	158.99	3.94
SO-13SD	07KNSTD	KNSTD	20.8268	0.2621	17276.00	676.00	12275.00	317.00	18.106	24.25	0.95	104.20	2.69
SO-2	07KNSTD	KNSTD	96.691	0.2595	14359.00	217.20	16641.00	434.50	14.307	4.30	0.07	23.81	0.62
SO-3	KNSTD	KNSTD	22.6952	0.2587	9343	176	38135	1848	2.651	10.59	0.23	42.90	2.08
SO-3R1	07KNSTD	KNSTD	35.134	0.2558	10086.00	211.60	13081.00	331.10	12.320	8.19	0.17	43.71	1.11
SO-3R2	07KNSTD	KNSTD	10.78	0.2554	3424.00	148.50	41135.00	1785.00	1.191	9.03	0.39	43.27	1.88
SO-3R4	07KNSTD	KNSTD	15.73	0.2547	5247.00	151.40	42057.00	1821.00	1.793	9.47	0.27	45.51	1.97
SO-3SD	KNSTD	KNSTD	13.0699	0.2569	3520	277	7063	1988	3.572	6.77	0.61	18.36	5.20
SO-4	07KNSTD	KNSTD	16.1871	0.2604	6484.00	316.20	16106.00	514.20	5.286	11.63	0.57	51.03	1.63

TABLE 2
(continued)

Sample name	assumed density (g cm^{-2})	Shielding correction	Be AMS standard	Al AMS standard	sample mass (g)	^{10}Be carrier (g)	$^{10}Be/^{9}Be_{measured}$ (x10^{-15})	± (x10^{-15})	$^{26}Al/^{27}Al_{measured}$	± (x10^{-15})	^{10}Be blank (x10^{-15})	^{26}Al blank (x10^{-15})	$Al/Be_{measured}$[2]
SO-4SD	KNSTD	KNSTD	13.0256	0.2562	3184	123	6661	569.6	5.972	6.11	0.27	28.96	2.49
SO-5	07KNSTD	KNSTD	17.489	0.2571	5356.00	126.20	10709.00	297.20	9.117	8.78	0.21	53.46	1.48
SO-6	KNSTD	KNSTD	13.2305	0.2593	19959	799	38671	1604	6.100	39.11	1.75	172.11	7.15
SO-6SD	KNSTD	KNSTD	7.7488	0.259	4672	144	10472	379.5	6.004	15.38	0.54	77.99	2.84
SO-6WA	07KNSTD	KNSTD	24.7393	0.2603	8625.00	390.10	14356.00	379.70	11.244	10.12	0.46	63.27	1.67
SO-7	07KNSTD	KNSTD	37.2733	0.2601	4984.00	252.50	8311.00	252.10	15.400	3.88	0.20	33.26	1.01
SO-8CH	KNSTD	KNSTD	12.794	0.2599	4039	116	8229	1034	5.532	8.06	0.27	34.27	4.33
SO-9CH	07KNSTD	KNSTD	23.9056	0.2588	7713.00	303.60	n/a	n/a	n/a	9.31	0.37	0.00	0.00
SOI-SD	KNSTD	KNSTD	36.1743	0.2569	9166	322	24225	1575	5.163	6.47	0.26	33.04	2.15

[1] Processed at Australian Nuclear Science and Technology Laboratory.

Table 3

Cosmogenic nuclide concentrations

Sample name	scaled [^{10}Be]^{1} Lal/Stone (2000)	error (1σ analytical)	[^{26}Al]/[^{10}Be]	error (1σ analytical)	Erosion rate (m/Ma) Lal/Stone (2000)	± (2σ external)	Age (Ma) Lal/Stone (2000)	± (2σ external)
BA-10SD	2.63	0.11	6.03	0.41	0.76	0.11	0.69	0.08
BA-11	7.18	0.21	n/a	n/a	0.07	0.03	3.29	0.78
BA-11#2	6.31	0.24	4.51	0.21	0.13	0.04	2.46	0.46
BA-12SDL	3.52	0.11	4.89	0.69	0.48	0.07	1.00	0.12
BA-12SDsm	4.64	0.08	4.95	0.18	0.28	0.05	1.46	0.19
BA-13CHL	5.44	0.18	4.47	0.64	0.20	0.05	1.88	0.29
BA-13CHsm	5.69	0.10	4.25	0.28	0.17	0.04	2.03	0.32
BA-13SD	7.27	0.17	5.22	0.31	0.07	0.03	3.40	0.82
BA-15CH	3.74	0.16	n/a	n/a	0.43	0.07	1.08	0.14
BA-16	4.12	0.07	5.63	0.20	0.35	0.06	1.23	0.15
BA-17CH	0.54	0.03	4.16	0.36	5.09	0.53	0.12	0.01
BA-18CH	1.19	0.21	6.68	1.19	2.04	0.47	0.28	0.06
BA-22CH	0.10	0.01	5.54	0.48	30.09	3.22	0.02	0.00
BA-23QC	0.59	0.04	6.42	0.62	5.80	0.63	0.14	1.52
BA-23sm	0.48	0.10	8.20	2.69	7.45	1.97	0.11	0.03
BA-24sm	2.78	0.51	8.53	1.81	11.46	2.55	0.74	0.02
BA-25A	0.41	0.02	6.60	0.61	7.78	0.69	0.09	0.01
BA-25B	0.75	0.03	7.37	0.43	3.94	0.37	0.17	0.02
BA-25C	1.56	0.05	6.22	0.63	1.59	0.17	0.38	0.04
BA-25CH	1.66	0.08	5.60	1.45	1.45	0.17	0.41	0.05
BA-27A	5.32	0.12	4.19	0.32	0.21	0.05	1.81	0.27
BA-27CH	3.96	0.12	3.96	0.23	0.40	0.06	1.17	0.15
BA-27CH	3.93	0.12	3.96	0.23	0.40	0.06	1.16	0.14
BA-2CH	2.23	0.04	3.11	0.42	0.94	0.11	0.57	0.06
BA-2SD	1.96	0.07	6.47	0.33	1.11	0.13	0.49	0.05
BA-3	4.31	0.13	5.19	0.20	0.33	0.06	1.31	0.17
BA-4	3.49	0.10	n/a	n/a	0.49	0.07	0.99	0.12
BA-4SD	2.27	0.12	5.38	0.34	0.94	0.12	0.58	0.07
BA-5	7.44	0.19	4.54	0.21	0.06	0.03	3.62	0.95
BA-5SD	2.83	0.09	4.98	0.27	0.68	0.09	0.76	0.09

TABLE 3
(continued)

Sample name	scaled [^{10}Be][1] Lal/Stone (2000)	error (1σ analytical)	[^{26}Al]/[^{10}Be]	error (1σ analytical)	Erosion rate (m/Ma) Lal/Stone (2000)	± (2σ external)	Age (Ma) Lal/Stone (2000)	± (2σ external)
BA-6	10.56	0.12	3.31	0.16	saturated	saturated	saturated	saturated
BA-6R1	6.96	0.20	2.62	0.11	0.09	0.03	3.05	0.66
BA-6R2	7.49	0.33	4.11	0.29	0.06	0.03	3.70	1.05
BA-6SD	5.09	0.23	3.93	0.26	0.24	0.05	1.68	0.26
BA-7	0.87	0.01	2.58	0.08	2.98	0.27	0.20	0.02
BA-8	0.76	0.04	n/a	n/a	3.76	0.39	0.18	0.02
BA-8A	1.45	0.07	5.44	0.29	1.78	0.20	0.35	0.04
BA-9	3.71	0.18	4.83	0.28	0.47	0.08	1.07	0.14
BA-9A	4.45	0.27	4.87	0.32	0.33	..07	1.38	0.21
BU-4	9.26	0.22	3.88	0.20	saturated	saturated	saturated	saturated
CA-1CH	1.07	0.07	n/a	n/a	2.31	0.28	0.25	0.03
CA-1SD	1.19	0.04	6.31	0.27	2.04	0.21	0.28	0.03
CRE-1	3.44	0.30	5.43	0.52	0.49	0.10	0.97	0.15
CRE-2	2.74	0.07	5.37	0.41	0.71	0.09	0.73	0.08
CRE-4	2.97	0.08	6.01	0.46	0.62	0.08	0.81	0.09
CRE-5	3.64	0.05	3.37	0.14	0.45	0.06	1.04	0.12
CRE-6	3.11	0.05	2.40	0.08	0.58	0.08	0.85	0.09
CRE-7	2.91	0.14	6.42	0.26	0.64	0.09	0.79	0.10
CRE-8	3.36	0.07	5.35	0.28	0.51	0.07	0.94	0.11
CRW-1	0.05	0.03	n/a	n/a	88.89	29.15	0.01	0.01
CRW-2	0.07	0.02	6.94	2.13	61.90	15.20	0.02	0.00
CRW-3	0.35	0.09	3.60	1.32	10.51	3.18	0.08	0.02
CRW-4	0.61	0.05	6.00	0.55	5.62	0.66	0.14	0.02
CRW-5	0.04	0.01	10.28	6.90	111.93	23.49	0.01	0.00
CRW-7	1.08	0.10	7.10	0.82	2.47	0.36	0.26	0.04
CRW-8	1.47	0.05	6.48	0.51	1.70	0.18	0.36	0.04
CT-50	3.36	0.06	5.62	0.15	0.52	0.07	0.94	0.11
CT-51	3.99	0.11	7.10	0.57	0.38	0.06	1.18	0.15
CT-52	2.55	0.09	5.64	0.26	0.78	0.10	0.67	0.75
CT-53	3.72	0.16	6.06	0.33	0.43	0.07	1.07	0.14

Table 3
(continued)

Sample name	scaled [^{10}Be]^{1} Lal/Stone (2000)	error (1σ analytical)	[^{26}Al]/[^{10}Be]	error (1σ analytical)	Erosion rate (m/Ma) Lal/Stone (2000)	± (2σ external)	Age (Ma) Lal/Stone (2000)	± (2σ external)
CT-54	3.00	0.12	6.25	0.33	0.62	0.09	0.81	0.10
CT-55	1.95	0.07	8.56	1.03	1.13	0.13	0.49	0.05
CT-56	2.61	0.13	5.85	0.43	0.76	0.11	0.69	0.82
CT-57	8.59	0.68	5.60	0.60	0.74	0.12	7.10	0.10
CT-58	2.68	0.11	6.37	0.99	0.75	0.10	0.71	0.08
PC-1	5.10	0.23	5.18	1.36	0.23	0.05	1.69	0.26
PC-1A	3.95	0.18	5.20	0.36	0.40	0.07	1.16	0.16
PC-1SD	2.58	0.06	6.72	0.24	0.79	0.10	0.68	0.07
PC-2	2.74	0.15	5.69	0.35	0.73	0.10	0.73	0.09
PC-2A	2.25	0.09	7.76	0.80	0.98	0.12	0.58	0.06
PC-3	6.44	0.21	3.31	0.66	0.12	0.04	2.57	0.49
PC-3BR	3.69	0.13	6.93	0.55	0.45	0.07	1.06	0.13
PC-4	5.30	0.09	4.75	0.12	0.23	0.05	1.80	0.26
PC-5	4.96	0.21	n/a	n/a	0.25	0.05	1.62	0.24
PC-5SD	4.19	0.11	4.32	0.22	0.36	0.06	1.26	0.16
PC-6	2.56	0.12	6.92	0.42	0.80	0.11	0.67	0.08
PC-7	3.03	0.10	5.62	0.33	0.62	0.08	0.82	0.10
S0-8BA	1.09	0.04	5.89	0.44	2.26	0.24	0.26	0.03
SA-1SD	1.93	0.14	5.10	1.18	1.14	0.16	0.48	0.06
SA-2CC	0.13	0.01	3.90	0.56	25.40	2.22	0.03	0.00
SA-2QC	0.09	0.01	6.87	0.33	39.61	4.40	0.02	0.00
SA-2SD	0.33	0.01	7.21	0.50	8.70	0.77	0.08	0.01
SA-3	0.07	0.00	8.10	0.74	45.54	4.79	0.02	0.00
SA-3SD	0.28	0.01	6.34	0.40	10.35	0.96	0.06	0.01
SA-4BD	0.70	0.22	3.10	1.02	3.81	1.54	0.16	0.06
SA-4CH	0.92	0.08	5.60	0.91	2.79	0.39	0.22	0.03
SO-1	6.01	0.23	4.92	0.32	0.15	0.04	2.24	0.39
SO-10SD	2.91	0.10	5.19	0.27	0.65	0.09	0.78	0.09
SO-11CH	5.42	0.19	n/a	n/a	0.20	0.05	1.87	0.29
SO-12	3.75	0.07	4.55	0.15	0.42	0.06	1.09	0.13

Table 3
(continued)

Sample name	scaled [^{10}Be]^{1} Lal/Stone (2000)	error (1σ analytical)	[^{26}Al]/[^{10}Be]	error (1σ analytical)	Erosion rate (m/Ma) Lal/Stone (2000)	± (2σ external)	Age (Ma) Lal/Stone (2000)	± (2σ external)
SO-13	3.88	0.16	7.21	0.35	0.39	0.07	1.14	0.15
SO-13SD	4.40	0.17	4.30	0.20	0.31	0.06	1.35	0.18
SO-2	2.45	0.04	5.54	0.17	0.85	0.10	0.64	0.07
SO-3	5.92	0.13	4.48	0.24	0.15	0.04	2.18	0.36
SO-3R1	5.18	0.11	5.34	0.18	0.23	0.05	1.74	0.25
SO-3R2	5.99	0.26	4.79	0.29	0.15	0.14	2.23	0.40
SO-3R4	5.80	0.17	4.81	0.25	0.17	0.14	2.10	0.34
SO-3SD	3.71	0.33	3.00	0.89	0.44	0.10	1.07	0.18
SO-4	7.39	0.36	4.39	0.25	0.06	0.04	3.56	0.98
SO-4SD	3.41	0.15	5.24	0.51	0.51	0.08	0.96	0.12
SO-5	4.22	0.10	6.09	0.22	0.35	0.06	1.28	0.16
SO-6	6.82	0.30	4.87	0.30	0.09	0.40	2.90	0.65
SO-6SD	2.62	0.09	5.61	0.28	0.74	0.10	0.69	0.01
SO-6WA	1.91	0.09	6.25	0.38	1.14	0.14	0.48	0.05
SO-7	0.78	0.04	n/a	n/a	3.61	0.38	0.18	0.02
SO-8CH	1.21	0.04	4.70	0.61	1.99	0.21	0.29	0.03
SO-9CH	4.61	0.18	n/a	n/a	0.29	0.06	1.45	0.20
SOI-SD	3.58	0.14	5.65	0.43	0.47	0.07	1.02	0.13

level, high latitude (SLHL) production rate of 4.5 atoms/gram/year. A $^{26}Al/^{10}Be$ production ratio of 6.8 (Balco and Rovey, 2008) is assumed.

Analytical Methods

Quartz was separated from samples and ^{10}Be and ^{26}Al isolated at the Purdue Rare Isotope Measurement (PRIME) Lab using standard methods modified after Kohl and Nishiizumi (1992). Sediment and crushed rock was sieved to the various grain sizes and the 0.25 mm or larger grain size was processed in order to exclude windblown contributions. All samples were purified to quartz with less than 450 ppm Al and were subjected to at least two 10 hour leaches in a warm 1 percent HF/HNO_3 solution in an ultrasonic bath to ensure removal of all meteoric ^{10}Be. The resulting clean quartz was spiked with ~250 μg of ^{9}Be in a weak HNO_3 carrier solution. The quartz was then subjected to ion chromatography methods after von Blanckenburg and others (1996). Samples were loaded into quartz crucibles, dried, and then calcined at 1100 °C for one hour. The oxides were then crushed and mixed with either niobium powder (Be) or silver powder (Al), and loaded into stainless steel holders for analysis by accelerator mass spectrometry (AMS). AMS measurements were made at PRIME Lab against standards prepared by K. Nishiizumi (Nishiizumi and others, 2007). Stable aluminum concentrations were determined by ICP-OES.

Environmental Variables

Precipitation data are scarce across the Atacama and unavailable at any particular sample site. We obtained the precipitation data in table 1 by interpolating between precipitation data stations (worldclimate.com). Interpolations were aided by observations of nitrate soils and the distribution of vegetation. The minimum value required to support perennial vegetation is considered to be 50mm/yr. The value for nitrate soils is assumed to be 0.1 mm/yr.

TRANSECT FEATURES

The Western Coastal Cordillera

The area immediately adjacent (<1km) to the coast consists of the coastal escarpment (up to 3000 m high), the coastal plain, the coastal rise, and the beach (fig. 5). The coastal plain consists of up to 500 m of thick, coarse-grained sediment. Coalesced alluvial fans and recent debris flows are prominent features on the coastal plain (fig. 5C). Lomas vegetation, consisting of annuals, perennial shrubs, and cactus, is sustained principally by fog-derived moisture and covers escarpment slopes up to an elevation of ~1000 meters above sea level (m asl). The coastal rise consists of a small (<30 m), steep rise located above the beach. In general, bedrock is not exposed along the coastal plain, but is occasionally observed at the top of the coastal rise.

The concentration of normalized ^{10}Be in sediments systematically decreases between the coastal rise and the coastal escarpment (fig. 5D). Sediments at the base of the coastal escarpment (~220 m asl) have normalized ^{10}Be concentrations of $0.05 \pm 0.03 \times 10^6$ atoms/gram. In contrast, sediments ~100 meters above the Pacific have normalized ^{10}Be concentrations between 0.35 and 0.59×10^6 atoms/gram. Bedrock exposed 24 meters above the ocean has a normalized ^{10}Be concentration of $0.61 \pm 0.05 \times 10^6$ atoms/gram.

The Eastern Coastal Cordillera

The Coastal Cordillera rises up to 3000 m asl and is characterized by precipitation rates that decrease sharply with distance from the ocean. For example, relatively abundant, fog-supported lomas vegetation transitions to absolute desert over a distance of <30 km. Exposed bedrock and gypsum-rich soils are present in the largely

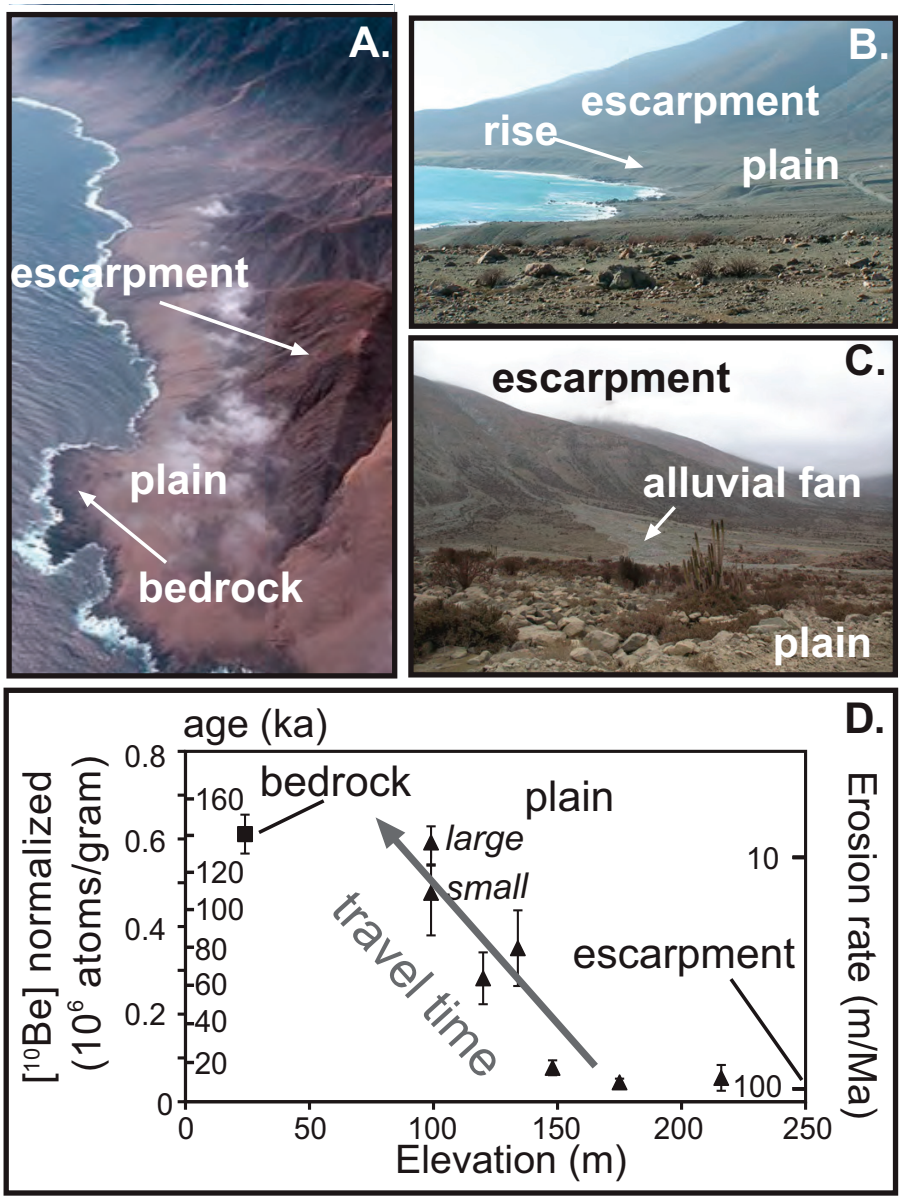

Fig. 5. Major features of the Coastal Cordillera. (A) The escarpment, coastal plain, and exposed bedrock. (B) The coastal rise, coastal plain, and escarpment. (C) The escarpment, alluvial fan, and coastal plain. (D) Normalized ^{10}Be concentrations and corresponding exposure ages and erosion rates across the coastal plain. Samples of channel sediments are represented by triangles and the bedrock sample is represented by a square. The gray arrow designates additional cosmogenic nuclides acquired in transit across the coastal plain.

plantless eastern Coastal Cordillera. Valleys to the east are filled with sand and colluvium and evidence of recent alluvial activity diminishes. Topography is steep throughout the Coastal Cordillera and active fault scarps are visible, particularly in association with the Atacama fault zone (AFZ).

The normalized concentrations of cosmogenic nuclides in the Coastal Cordillera increase in all types of sediment with distance from the Pacific. The portion of the coastal range that is within the absolute desert has normalized ^{10}Be concentrations as high as 5.32×10^6 atoms/gram, some of the highest normalized ^{10}Be concentrations observed in this data set. In addition to east-west transects across the Coastal Cordillera, our sampling effort focused on a north-south transect of bedrock and sediment samples along the western side of the AFZ; samples in this transect have a relatively narrow range of concentrations, ranging between 2.74 and 3.44×10^6 atoms/gram (fig. 6C).

A site that typifies the eastern Coastal Cordillera is site 1, located less than 12 km from the coast and east of the main drainage divide (fig. 7A). At this location the Coastal Cordillera has a relatively low elevation (max ~1500 m asl) and the AFZ consists of multiple splays, which create a series of small north-south trending basins (fig. 7A). The width of the interior basin is ~3.5 km, with a base elevation of ~ 800 m. Incised drainage networks are visible on both sides of the basin. On the western side of the basin, sufficient precipitation near the head of an alluvial fan allows intermittent growth of woody vegetation. Modern flowing water on the head of this fan is evidenced by small gravel bars located behind this dead wood. In contrast, the eastern side of this basin has sparse, inactive drainages.

Normalized concentrations of ^{10}Be in both boulders and sediments rapidly increase to the east at Site 1 (fig. 7D). The normalized concentration of ^{10}Be in sediment on the west side of the basin is $0.65 \pm 0.16 \times 10^6$ atoms/gram; on the east side of the basin this concentration is 3.96×10^6 atoms/gram. In the center of the valley, the normalized concentration of ^{10}Be in fluvial sediment is $1.48 \pm 0.08 \times 10^6$ atoms/gram. The westernmost boulder here has a normalized ^{10}Be concentration of $0.41 \pm 0.02 \times 10^6$ atoms/gram. Boulders further east have normalized ^{10}Be concentrations of 0.75 ± 0.03 and $1.56 \pm 0.05 \times 10^6$ atoms/gram. A quartz cobble exposed on the eastern side of the basin has a normalized ^{10}Be concentration of $5.32 \pm 0.12 \times 10^6$ atoms/gram.

The Absolute Desert

The Central Depression forms the core of the absolute desert. Almost all landforms in the Central Depression are mantled by a thick cover of loess and gypsum and hillslopes have gentle slopes. Thick sediments, which include significant deposits of loess and airfall tuff (Placzek and others, 2009b) fill valleys in the Central Depression. Even within the nitrate soil zone, raindrop imprints, mudcracks, and evidence of occasional water flow are observed.

A feature unique to the absolute desert is boulder fields. These fields include hundreds to thousands of individual boulders. Boulders are up to three meters in diameter and are generally found downslope of exposed bedrock. These boulders often cluster into continuous fields at the foot of hills and seismically smoothed surfaces on the sides of these boulders are described elsewhere (Quade and others, 2012). Boulder fields may be adjacent to more geomorphically active features such as washes that show evidence of recent movement of finer grained material. In addition to boulder fields, smaller boulders (diameter generally <0.75 m) and cobbles may be present on the surface of alluvial fans.

Site 2 is situated at an elevation of ~1000 m asl, and is located just east of the Coastal Cordillera (fig. 1B). The highest normalized ^{10}Be concentrations ($4.96 \pm 0.21 \times 10^6$; $5.10 \pm 0.23 \times 10^6$; $5.30 \pm 0.09 \times 10^6$; and $6.44 \pm 0.21 \times 10^6$ atoms/gram) at this site are found in the boulders located furthest downslope (fig. 8B). The lowest normalized ^{10}Be concentrations ($2.74 \pm 0.15 \times 10^6$; $2.25 \pm 0.09 \times 10^6$; and $2.74 \pm 0.15 \times 10^6$ atoms/gram) at this site are from surface sediments and boulders located at mid-hillslope. Bedrock and additional boulders at this site have intermediate normal-

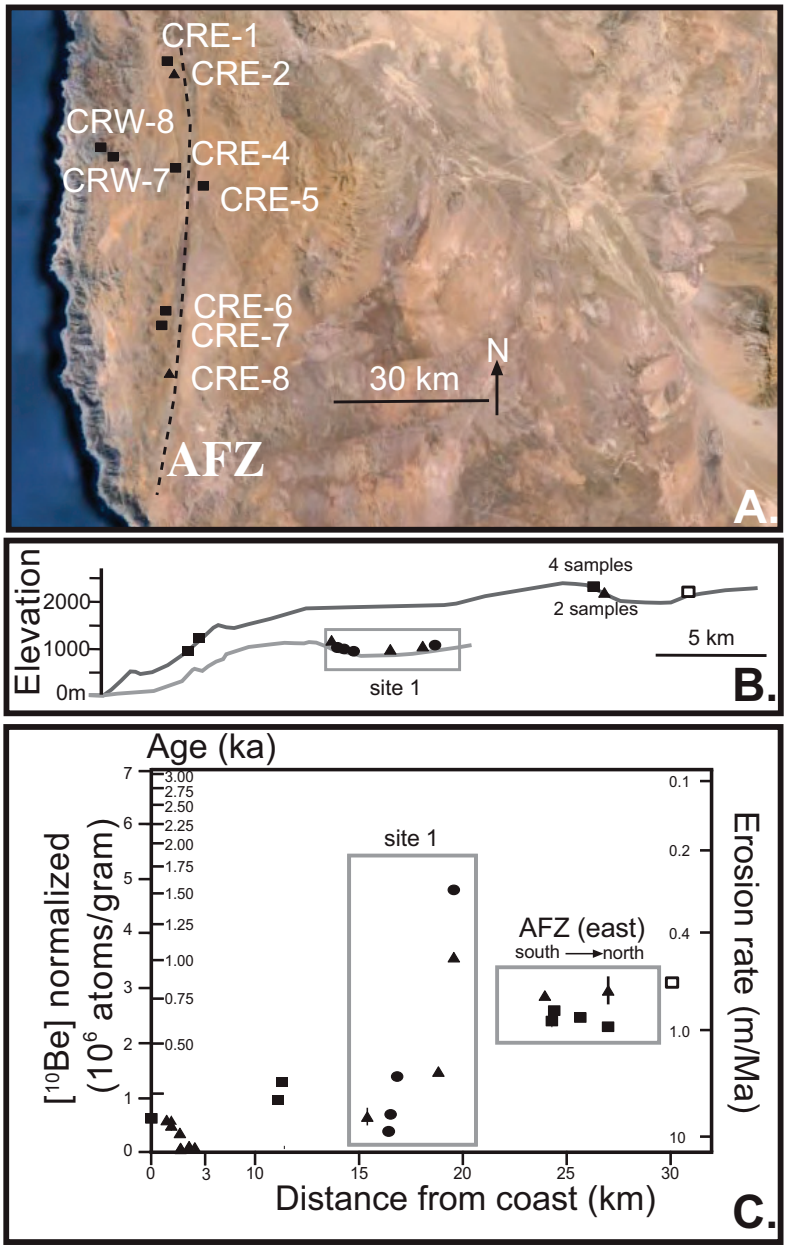

Fig. 6. Major features of interior Coastal Cordillera. (A) The location and types of samples within the Coastal Cordillera and from the southern transect (see fig. 7 for Site 1 details). Samples of channel sediments are represented by triangles and bedrock are represented by squares. The open square designates a bedrock sample with a burial signature. The Atacama Fault Zone (AFZ) is designated by a dashed line. See figure 7 for Site 1 details. (B) Elevation profiles of samples from the Coastal Cordillera. (C) Normalized ^{10}Be concentrations and corresponding exposure ages and erosion rates across the Coastal Cordillera. Symbols as in (B).

ized ^{10}Be concentrations of 3.69 ± 0.13 × 10^6; 3.96 ± 0.12 × 10^6 ; 4.19 ± 0.11 × 10^6atoms/gram, respectively.

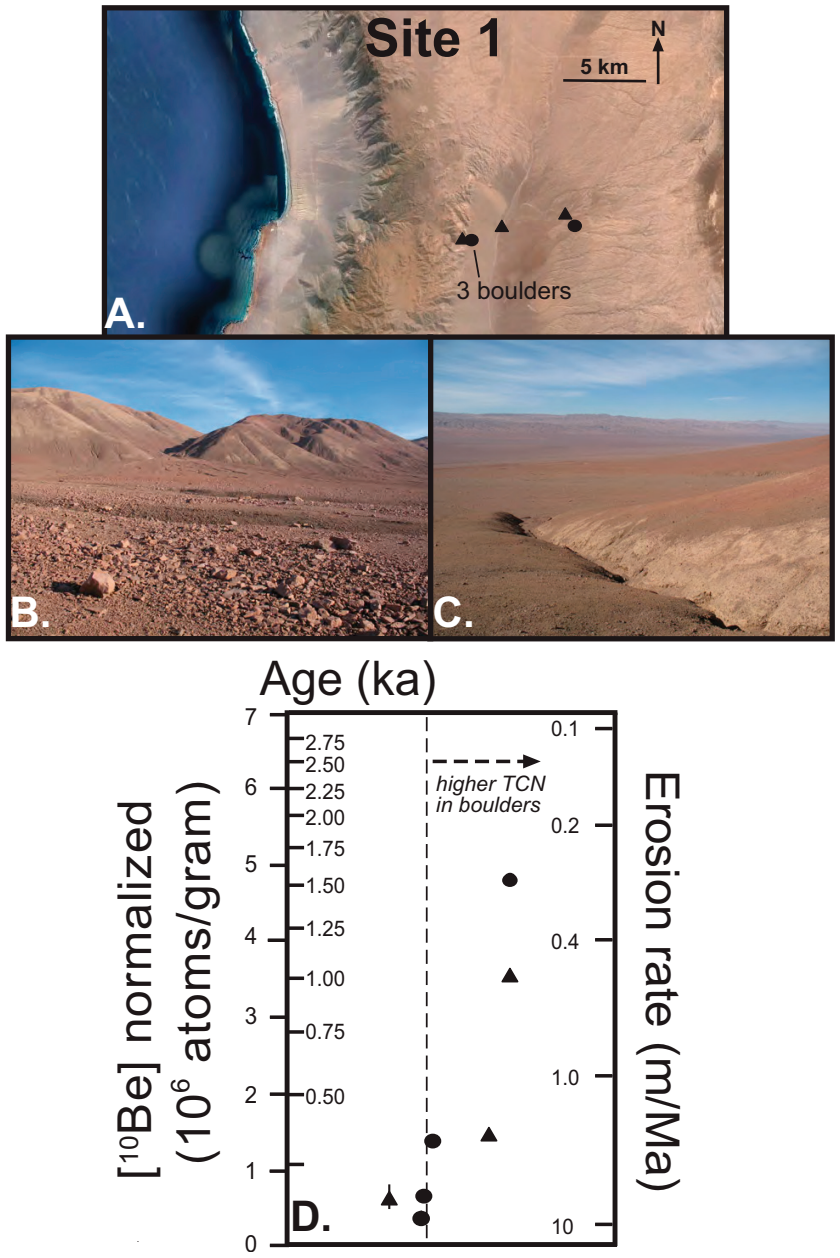

Fig. 7. Major features of Site 1. (A) The location and types of samples from site 1. Samples of channel sediments are represented by triangles and boulders/cobbles are represented by circles. (B) The west side of site 1. Note active alluvial fans; dead perennial vegetation is present at the apex of this fan. (C) The east side of site 1, which has inactive drainages. (D) Normalized ^{10}Be concentrations and corresponding exposure ages and erosion rates across site 1. Symbols as in (A). The dashed line and arrow designates the zone where terrestrial cosmogenic nuclide concentations (TCN) are higher in boulders relative to sediments.

Near Site 2, several isolated mountain ranges stand over one kilometer above the landscape. We focused on one of these ranges, the Cerro de los Tetas, which is located

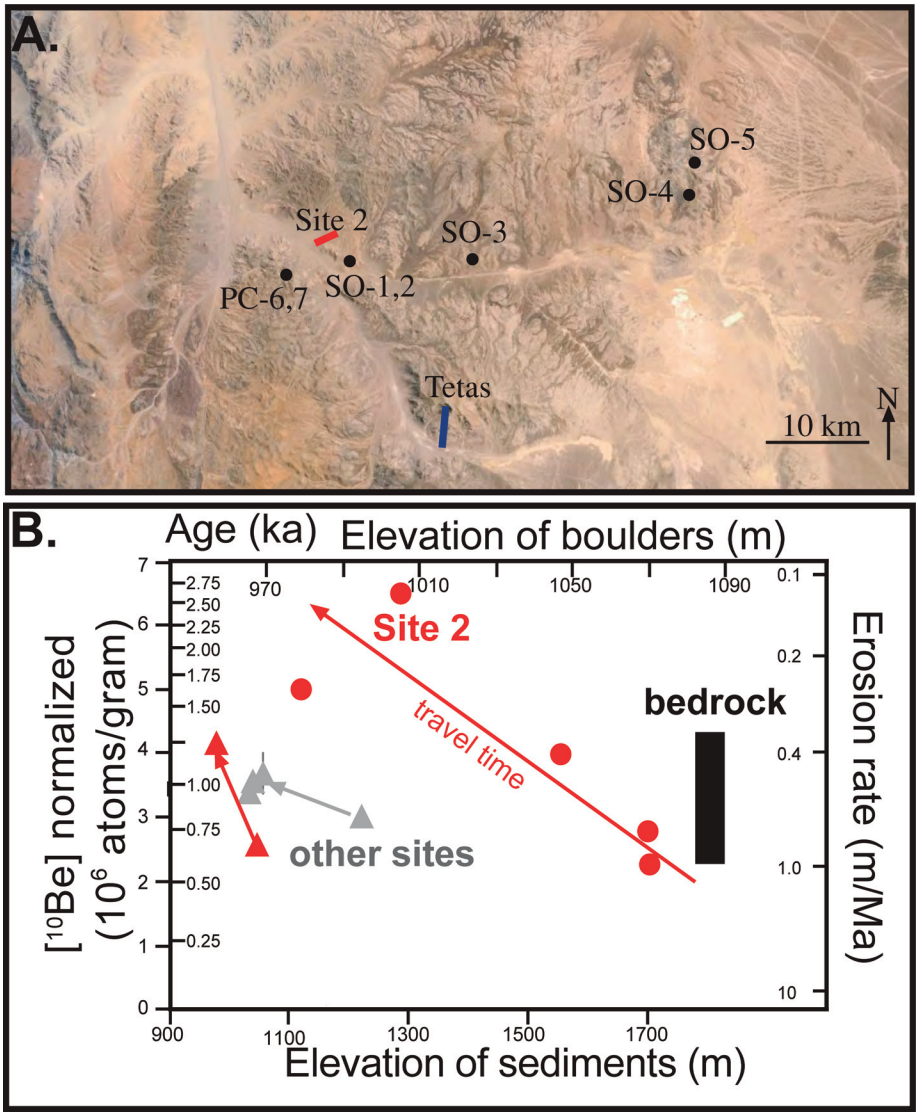

Fig. 8. Major features of the region around the Cerros de los Tetas. (A) The location of samples within the region; multiple sample types are present at each site. Site 2 consists of a downslope transect of boulders and sediments. (B) Normalized ^{10}Be concentrations and corresponding exposure ages and erosion rates plotted against elevation for the region. Bedrock samples are shown as the black bar and are not shown as a function of elevation. A downslope increase in ^{10}Be is particularly pronounced in boulders at Site 2 (red symbols); this trend is attributed to ^{10}Be acquired in transit–a trend indicated by the red lines.

in close proximity to Site 2. This granitic to dioritic mountain range is located east of the AFZ and reaches elevations of ~2200 m (fig. 7A). In contrast to the eastern Coastal Cordillera and Central Depression, bedrock is frequently exposed in the Tetas. Sparse perennial vegetation is infrequently present near the crest (fig. 9A), indicating somewhat higher precipitation. Topography is steep and active fault scarps are visible. Active alluvial drainages discharge around the bases of the Tetas.

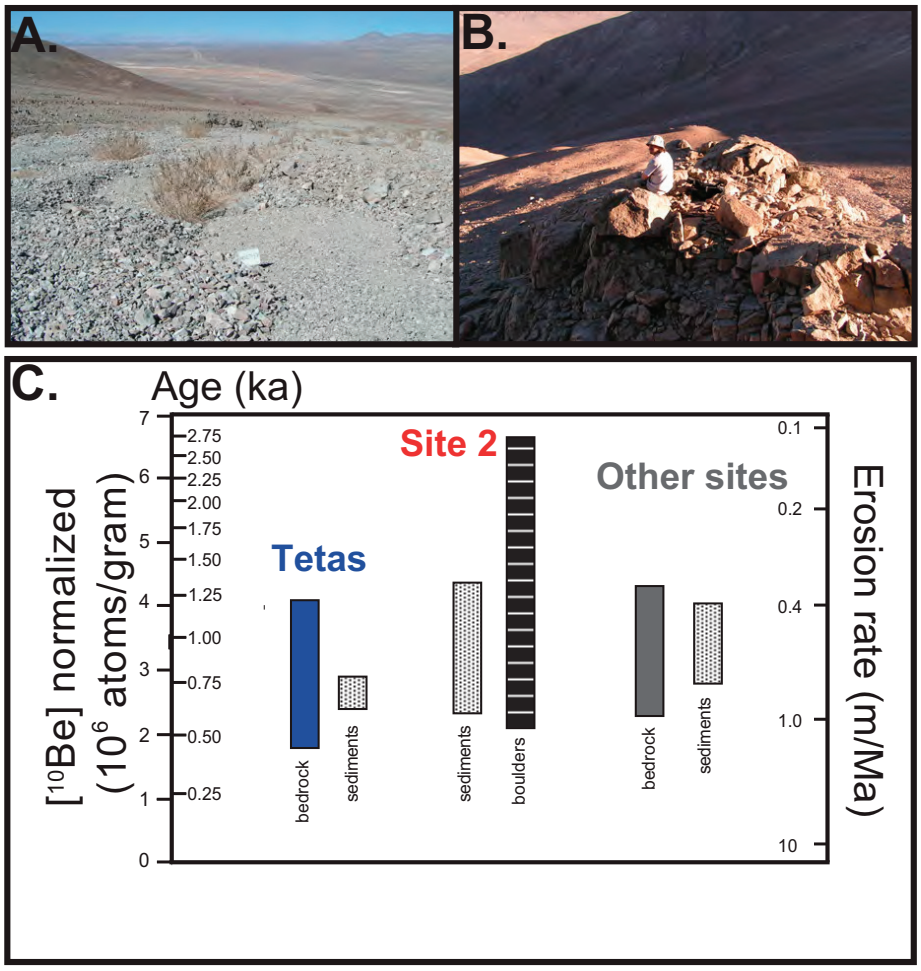

Fig. 9. Major features of Cerros de los Tetas and surrounding regions. (A) Vegetation and (B) bedrock are both exposed at the crest of these mountains. (C) Normalized ^{10}Be concentrations and corresponding exposure ages and erosion rates in the region surrounding the Cerros de los Tetas. All samples from the region have similar normalized ^{10}Be concentrations, with the exception of boulder samples that have higher normalized ^{10}Be concentrations.

The Cerro de los Tetas are characterized by relatively uniform cosmogenic nuclide concentrations. Most samples from the Cerro de los Tetas are bedrock with normalized concentrations of ^{10}Be that range from 1.95 to 3.99 $\times$ 10^6 atoms/gram (fig. 9C). These concentrations do not vary systematically with sample elevation. A sediment sample from near the base of the mountains has a cosmogenic nuclide concentration of 2.34 $\times$ 10^6 atoms/gram, overlapping with the concentration observed in bedrock.

Site 3 is on the western flank of the Cordillera Domeyko at an elevation of ~1500 meters. Boulders furthest down the slope have the highest normalized ^{10}Be concentrations at this site (6.31 $\pm$ 0.24; 7.18 $\pm$ 0.21; 7.44 $\pm$ 0.19; and 9.26 $\pm$ 0.22 $\times$ 10^6 atoms/gram) (fig. 10C). Intermediate normalized concentrations of ^{10}Be occur in bedrock (4.31 $\pm$ 0.13 $\times$ 10^6 atoms/gram) and in a partially exposed boulder (3.48 $\pm$

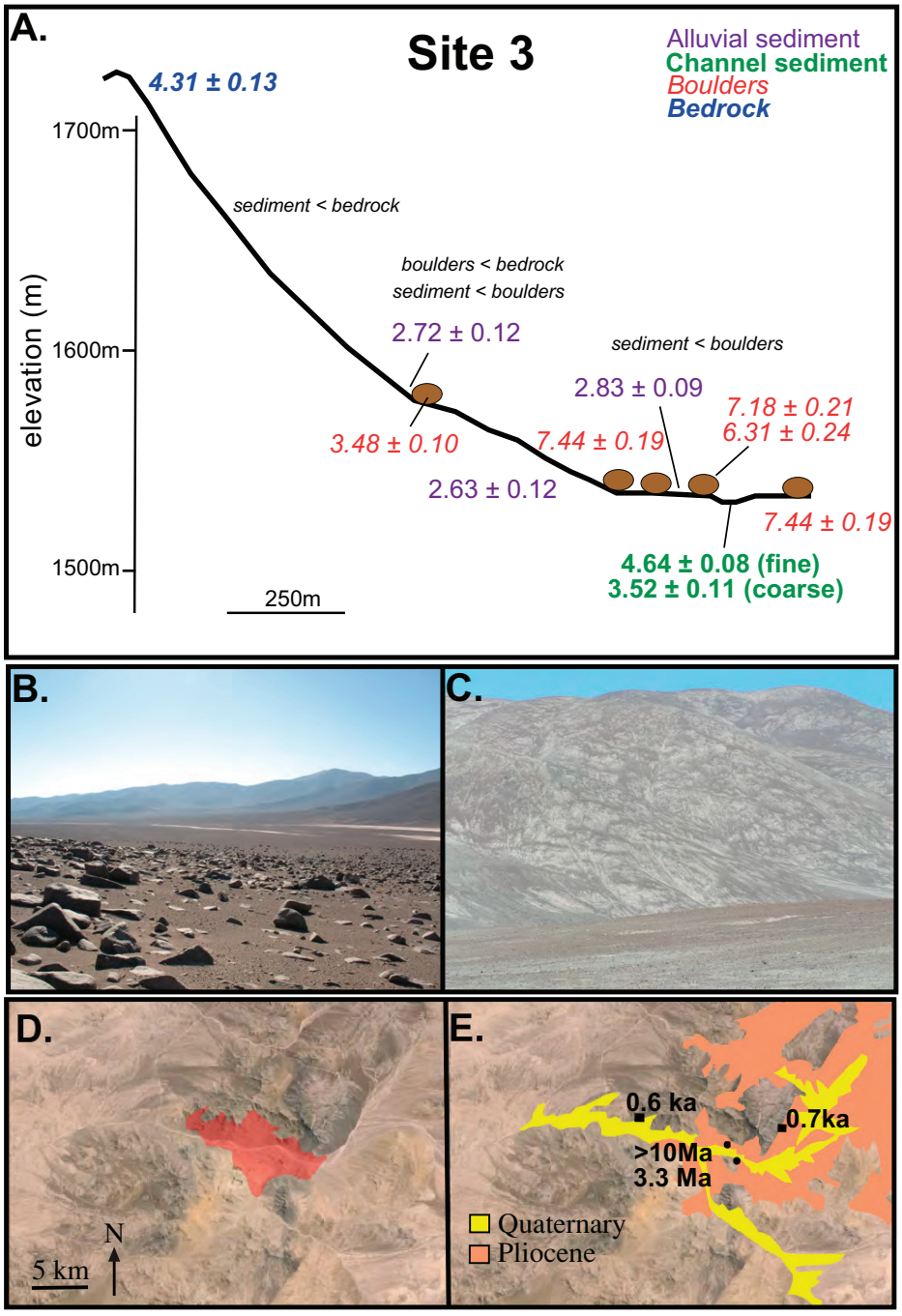

Fig. 10. (A) Normalized ^{10}Be concentrations ($\times 10^6$ atoms/gram) and features at and near Site 3. (B) Boulder field at Site 2. Boulders are up to 2 m in diameter. Old (>1 Ma) relict boulders are present in the foreground, but the dry wash in the background was recently active. (C) Chevroned lines of surface rock on a hillslope in the absolute desert near Site 2. (D) The region of site 2; the red shaded area inferred by Amundson and others (2012) to have 100–300 meters of Miocene to Pliocene incision, the maximum amount inferred in that study. (E) Quaternary (yellow) and Pliocene (pink) surfaces previously inferred for the region. Prior K-Ar ages are indicated and their locations are marked by black squares. New Miocene ages for boulders are indicated and the locations of the two oldest boulders are marked by black circles. In light of the new ages, the surfaces is much older than previously inferred and Miocene to Pliocene incision is much less than previously inferred.

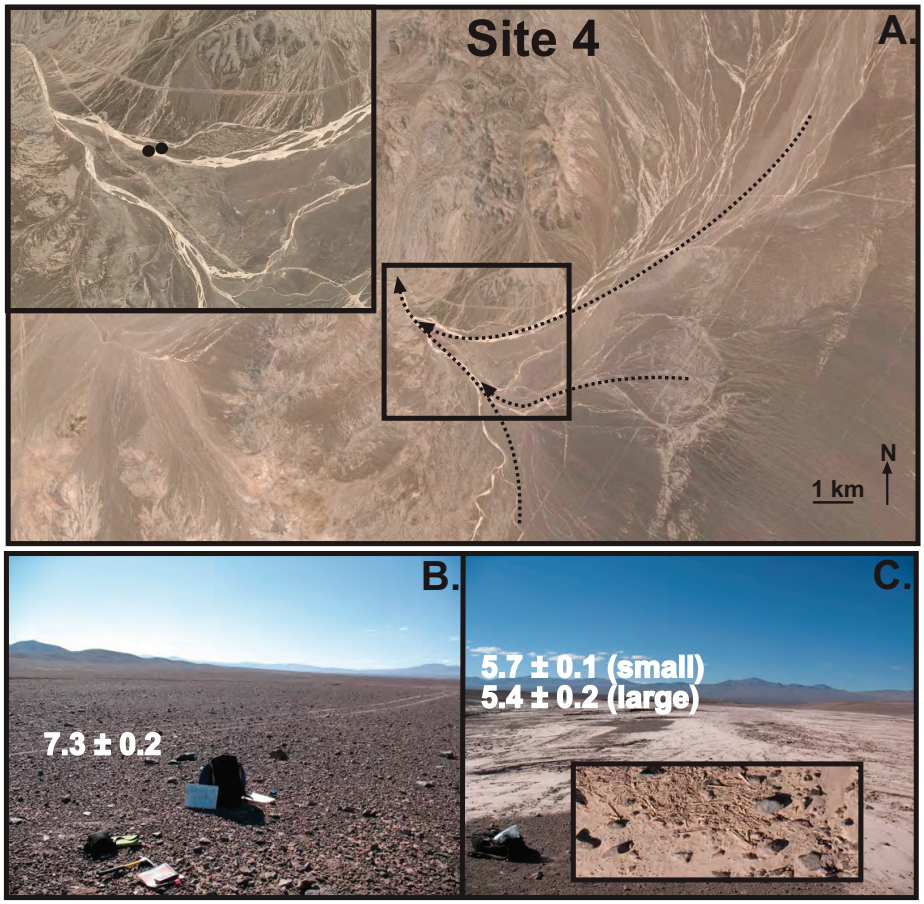

Fig. 11. Major features of Site 4. (A) Location of Site 4 within the absolute desert. Ephemeral washes (dashed lines) from the Cordillera Domeyko flow past the site. (B) The stable alluvial surface at the site and normalized ^{10}Be concentrations ($\times 10^6$ atoms/gram). (C). The wash that flows past the site with normalized ^{10}Be concentrations ($\times 10^6$ atoms/gram) indicated. Dry vegetation (inset) transported from higher elevation is present.

0.10×10^6 atoms/gram) located on the steep hillslope. The lowest normalized concentrations of ^{10}Be at this site occur in surface sediments, and range between $2.63 \pm 0.12 \times 10^6$ and $2.83 \pm 0.09 \times 10^6$ atoms/gram. Sediment in the axial channel of this drainage has a normalized concentration of $4.64 \pm 0.08 \times 10^6$ atoms/gram in the finest (0.25-0.5 mm) grain size fraction and a concentration of $3.52 \pm 0.11 \times 10^6$ in the coarse (>1 mm) fraction (fig. 10A).

Site 4 consists of a stable alluvial surface that is cut by recently active fluvial channels. This site is very sensitive to reworking due to wetter conditions in the Cordillera Domeyko, as dry washes headed in the Cordillera Domeyko have dissected this fan on both sides (fig. 11A). Plant debris is observed in this drainage (fig. 11C), documenting transport of material from regions with greater precipitation located at higher elevation. Furthermore, any significant influx of sediment from the adjacent hillsope will wash over this deposit (fig. 11A). The stable surface has developed a desert pavement (fig. 11B). This is one of the few desert pavements observed in the Atacama and has a normalized ^{10}Be of $7.27 \pm 0.17 \times 10^6$ atoms/gram. Sediment in the channel

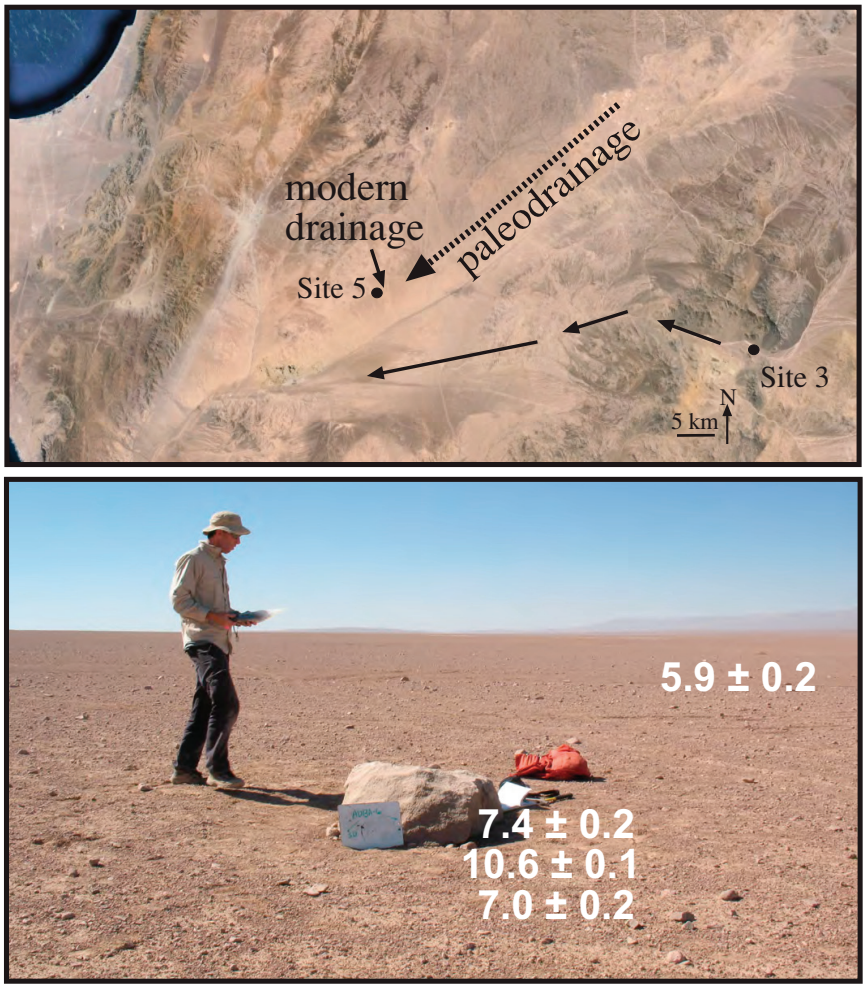

Fig. 12. Major features of Site 5. (A) Location of Site 5 within the absolute desert. Ephemeral modern washes (sold line) from the Coastal Cordillera flow past the site, but palaodrainage (dashed line) may have been from a different direction. (B) The stable alluvial surface at the site corresponding normalized ^{10}Be concentrations ($\times 10^6$ atoms/gram). Note the low slope of this site.

of the drainage has a normalized ^{10}Be concentration of $5.69 \pm 0.10 \times 10^6$ atoms/gram in the finest (0.25-0.5 mm) grain size fraction and $5.44 \pm 0.18 \times 10^6$ in the coarse (>1 mm) fraction.

Site 5 is located within the Central Depression in close proximity to the Coastal Cordillera. Modern drainage at this site is sourced from the eastern Coastal Cordillera, but paleodrainage may have come from further east (fig. 12A). This site hosts boulders with high normalized ^{10}Be concentrations. Concentrations of cosmogenic nuclides were analyzed from three different boulders at this site. The first boulder, BA-6, has one of the highest normalized concentration of ^{10}Be of all samples in this data set; the scaled ^{10}Be concentration ($10.56 \pm 0.12 \times 10^6$ atoms/gram) of this sample is saturated with respect to ^{10}Be production rates regardless of the chosen scaling factor. Samples BA-6R1 and BA-6R2 also have high normalized ^{10}Be concentration (6.96 ± 0.20 and

7.49 ± 0.33 × 10^6 atoms/gram, respectively); BA-6R2 has a $^{26}Al/^{10}Be$ ratio indicative of >1 Ma of burial. In contrast, finer-grained sediment at this site has a normalized ^{10}Be concentration of 5.09 ± 0.23 × 10^6 atoms/gram.

The Cordillera Domeyko

The crest of the Cordillera Domeyko averages over 3000 m with peaks rising above 4000 meters. The western flank of the Cordillera Domeyko is in the absolute desert and has features similar to the adjacent Central Depression. Near the western crest of the Cordillera Domeyko, active alluvial fans and channels occur; visible rilling is present and bedrock is occasionally exposed. Vegetation, indicative of higher rainfall, is present only near the crest of the Cordillera Domeyko, which is relatively flat. The western Cordillera Domeyko is characterized by steeply sloping, broad alluvial fans. The eastern Cordillera Domeyko is characterized by high relief and drops steeply into lower elevation saltpans. Steeply tilted, coarse sediments and gravels are also exposed on the eastern flank of the Cordillera Domeyko.

Normalized concentrations of ^{10}Be in the Cordillera Domeyko show significant spatial variability, with the eastern and western flanks having lower cosmogenic nuclide concentrations than the mountain crest (figs. 13 and 14). Concentrations of ^{10}Be near the crest of the Cordillera Domeyko range from 3.71 to 4.45 × 10^6 atoms/gram. Normalized concentrations of ^{10}Be in sediments from the eastern and western flanks of the Cordillera Domeyko range from 0.54 to 1.45 × 10^6 atoms/gram (figs. 13 and 14).

The Salars and the Andean Flank

The Cordillera Domeyko is flanked on the east by a series of large intermontane basins. In addition to the east-west transects across these salars, north-west transects along the western and eastern sides of these salars were sampled. Our sampling transects pass through the Salar de Atacama and Salar de Punta Negra, among the largest of these basins. Sediments derived from the Andean flank and Cordillera Domeyko empty onto these basins (figs. 13A and 14A). Active alluvial fan surfaces are present along the eastern fringes of salar basins. Boulders and cobbles at the foot of the Andean flank have normalized ^{10}Be concentrations between 0.09 and 0.70 × 10^6 atoms/gram; associated sediments have concentrations between 0.28 and 1.93 × 10^6 atoms/gram. In all types of sediment and on both sides of the salars, samples from the north have lower ^{10}Be concentrations than samples from the south (fig. 15A).

The Andean flank is characterized by both steep topography and a pronounced precipitation gradient associated with the SASM. Steep volcanic peaks in the region rise to greater than 6000 m asl. Ignimbrite sheets cover much of this region. Despite the high elevation of peaks, this region was not glaciated during the Last Local Glacial Maximum, as a result of extreme aridity (Ammann and others, 2001). Incised channels, often with perennial water, are present. Bedrock is frequently exposed. Rocky soils generally contain carbonate. Vegetation appears at elevations of 2500 to 3000 m and increases up to the 0°C isotherm (fig. 3). The normalized concentration of ^{10}Be in channels draining the Andes are between 0.096 and 1.19 × 10^6 atoms/gram and decrease with elevation (fig. 15B).

DISCUSSION

Evidence for Burial

Exposure-burial diagrams (fig. 4) indicate that most samples have concordant ^{10}Be and ^{26}Al concentrations, consistent with continuous exposure and/or steady erosion as predicted by equation 1. Other samples may also have minor burial periods, resulting in depressed $^{26}Al/^{10}Be$ ratios that overlap steady erosion within two sigma.

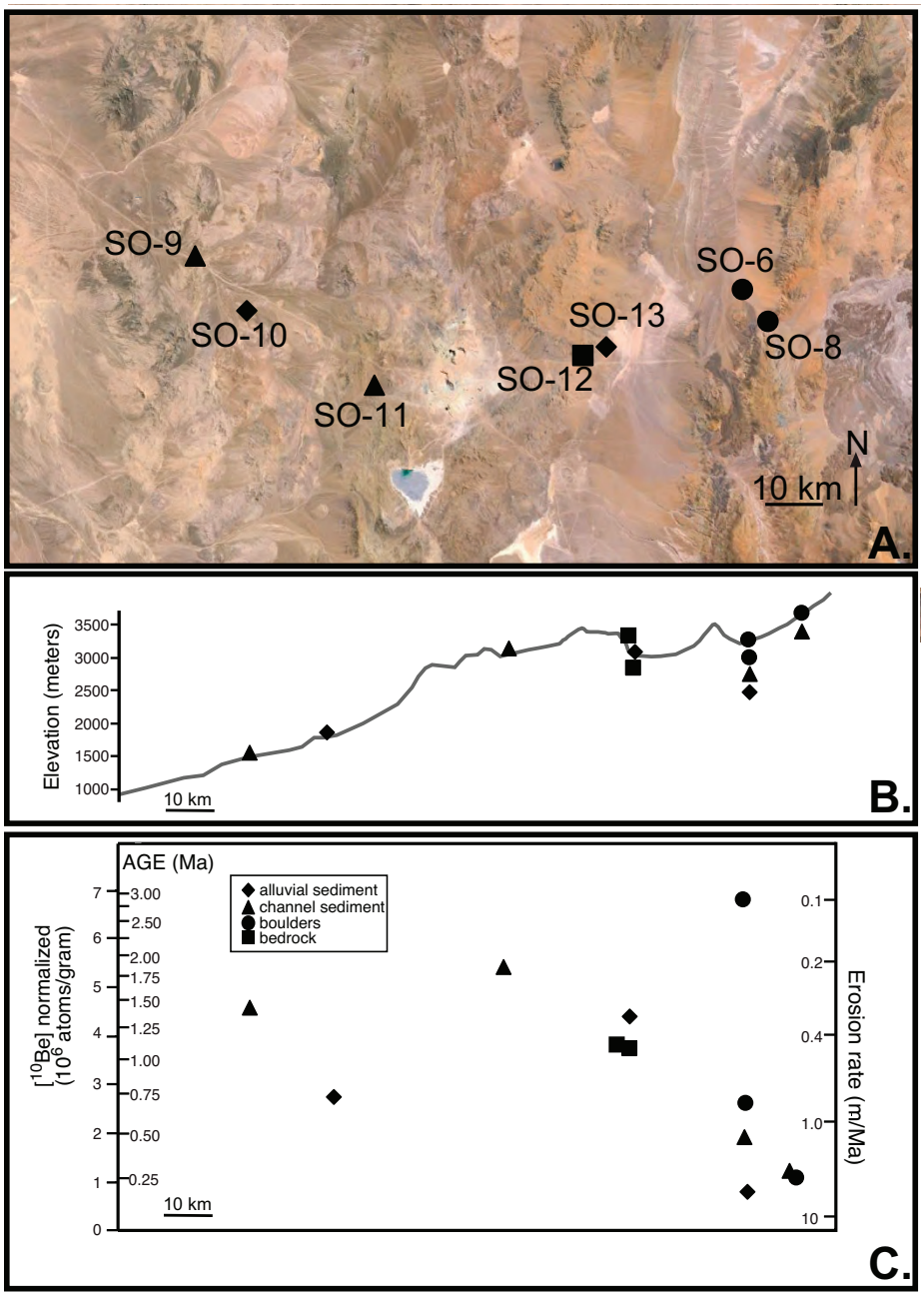

Fig. 13. (A) Major features of the southern transect across the Cordillera Domeyko and onto the Andean foothills. Samples of alluvial sediment are represented by diamonds, channel sediments by triangles, sites with multiple samples by circles, and bedrock by squares. (B) Elevation profiles of samples from this transect; symbols as in (A). (C) Normalized ^{10}Be concentrations and corresponding exposure ages and erosion rates for this transect; symbols as in (A).

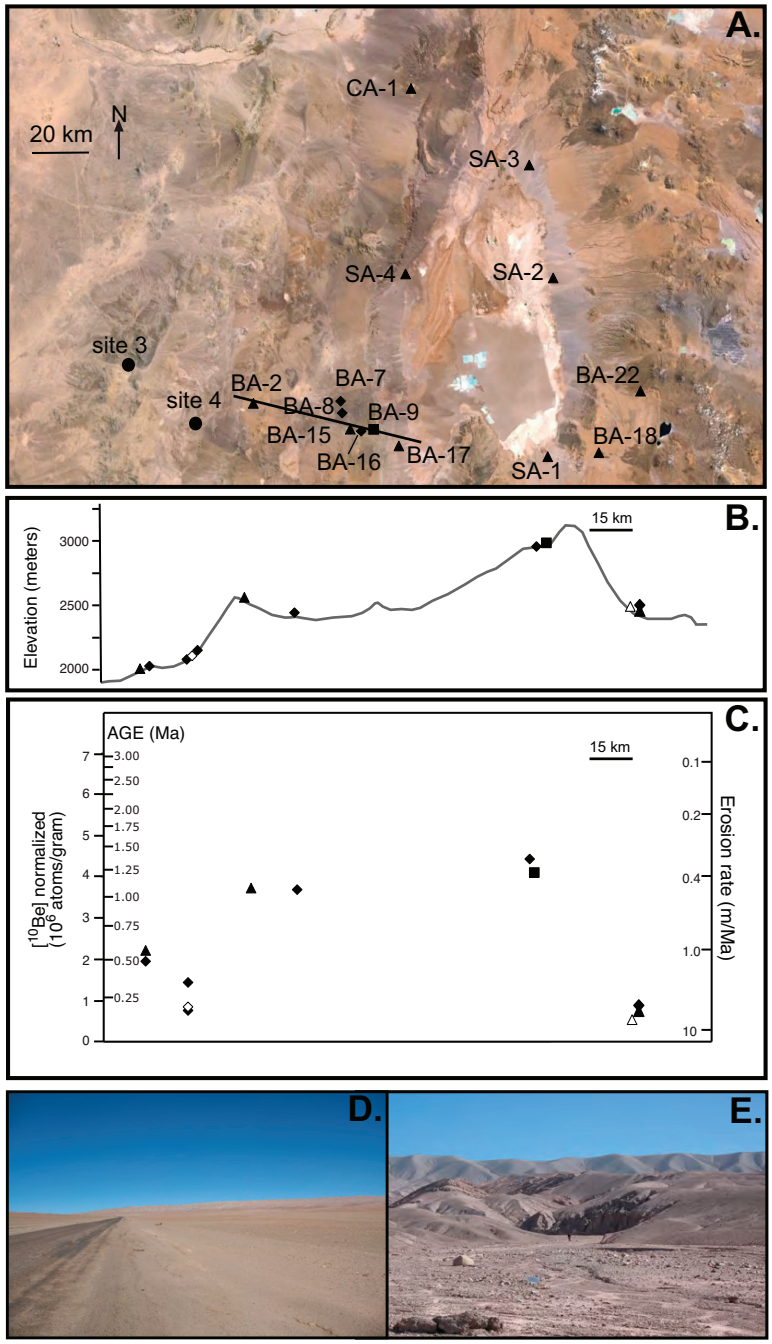

Fig. 14. (A) Major features of the northern transect across the Cordillera Domeyko and onto the Andean foothills. Samples of alluvial sediment are represented by diamonds, channel sediments by triangles, sites with multiple samples by circles, and bedrock by squares. Samples with a burial signature are represented by open symbols. (B) Elevation profiles of samples for the transect shown as a solid line in (A) ; symbols as in (A). (C) Normalized ^{10}Be concentrations and corresponding exposure ages and erosion rates for this transect; symbols as in (A). (D) The crest of the Cordillera Domeyko. (E) The eastern slope of the Cordillera Domeyko.

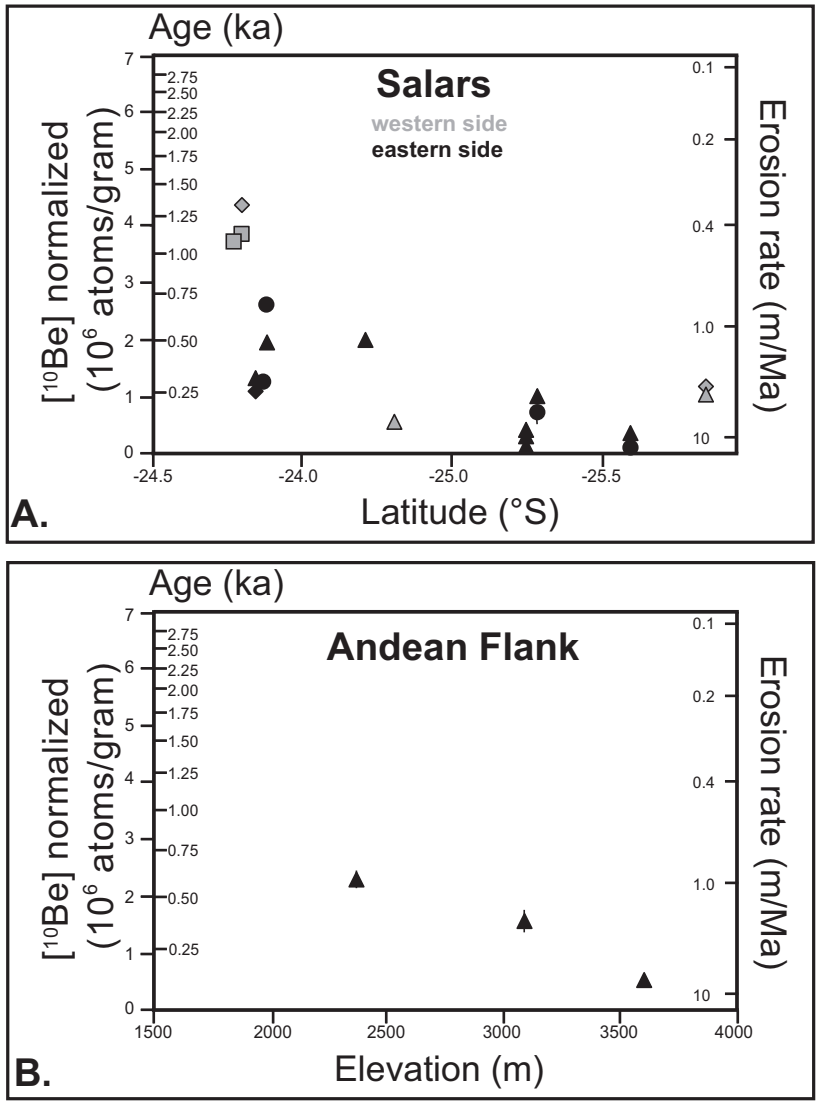

Fig. 15. (A) Normalized ^{10}Be concentrations and corresponding exposure ages and erosion rates verses latitude for samples from the Salars. Samples of alluvial sediment are represented by diamonds, channel sediments by triangles, sites with multiple samples by circles, and bedrock by squares. Black symbols are from the eastern side of the salars, gray symbols are from the western side. (B) Normalized ^{10}Be concentrations and corresponding exposure ages and erosion rates verses elevation for samples from the Andean flank.

Only seven samples have ^{26}Al/^{10}Be ratios exclusively indicative of significant burial. These samples occur throughout both transects and include one boulder with a very long exposure age (discussed in a subsequent section), two bedrock samples, two amalgamated quartz clast samples, and two samples of channel sediments.

Bedrock samples in this study sometimes have ^{26}Al/^{10}Be ratios indicative of a complex exposure history. Exposed bedrock in the central Atacama is rare and this exposed bedrock frequently consists of quartz veins, resembling that sampled as amalgamated quartz clasts. To that end, we suggest that the ^{26}Al/^{10}Be ratios indicative

of a complex exposure history for quartz clasts is likely inherited from bedrock. Owen and others (2011) inferred a complex exposure history from $^{26}Al/^{10}Be$ ratios for bedrock samples at four sites from the arid and hyperarid reaches of the Atacama. In contrast, Kober and others (2007) inferred steady-state erosion for most bedrock samples at 19 sites in the northern Atacama based on ratios of ^{26}Al, ^{10}Be, and ^{21}Ne. The results here suggest that complex exposure of bedrock is not a major process in the central Atacama; however, we suggest that it is a more significant process in the central Atacama than in the northern Atacama. The northern Atacama contrasts with the central Atacama in that bedrock is frequently exposed as massive ignimbrite sheets; whereas, exposed bedrock is rare in the central Atacama. We suggest that some bedrock samples in the central Atacama have $^{26}Al/^{10}Be$ ratios indicative of a complex exposure history due to episodic coverage by regolith. Mantling of the entire central Atacama by thick soils is the present day situation in the central Atacama, so these complex exposure histories do not imply a changing climate.

Two channel sediments in this study have $^{26}Al/^{10}Be$ ratios indicative of a complex exposure history, contrasting with previous studies that suggest a complex exposure history for Quaternary sediments from the northern Atacama. Most sediment samples from the Rio Lluta catchment in the northern Atacama have complex exposure histories revealed by ratios of the nuclides ^{26}Al, ^{10}Be, and ^{21}Ne (Kober and others, 2009). However, the Rio Lluta is significantly different from the channels sampled in this study in that it has perennial water and is also deeply incised with pronounced terraces.

Jungers and others (2013) report Quaternary sediments in two depth profiles in the central Atacama have $^{10}Be/^{21}Ne$ ratios indicative of a complex exposure history. These results, coupled with a Pliocene terrace that does not have $^{10}Be/^{21}Ne$ ratios indicative of a complex exposure history, are used to infer rapid sediment stripping under a wetter climate during the Pliocene (Jungers and others, 2013). The $^{26}Al/^{10}Be$ ratios reported here are much more sensitive to recent (Quaternary) burial than $^{10}Be/^{21}Ne$ ratios due to the shorter half-life of ^{26}Al. Indeed, $^{10}Be/^{21}Ne$ ratios will reveal a complex history if the rock has experienced prior exposure at any time or has undergone prolonged slow erosion in which ^{21}Ne was acquired during bedrock weathering (for example, Fujioka and others, 2005). The considerably expanded $^{26}Al/^{10}Be$ data set in this study suggests that surface sediments across the central Atacama do not generally have a complex history and that recycling of previously exposed sediments is not a major process in the central Atacama during the Quaternary.

Hillslope to Basin Cosmogenic Nuclide Concentrations

Slow geomorphic rates in a landscape are characterized by an interrelated combination of slow erosion rates, slow sediment transport rates, and geomorphic surfaces that are exposed for long periods of time. Here, hillslope transects from each sub-region of the Atacama Desert are examined to provide insights into sediment generation and transport. Several proposed landscape evolution models for the Atacama desert (Placzek and others, 2010; Amundson and others 2012; Quade and others 2012; Jungers and others, 2013) suggest that sediment is produced primarily on the hillslopes and then transported to basins by either sparse fluvial networks or across broad alluvial fans. In arid regions, a regular increase in cosmogenic nuclide concentration downslope reflects the slow transport of grains from hillslope sources to alluvial surfaces and ultimately to sinks where the sediments is stored (Nichols and others, 2002; Nichols and others, 2006). In the following sections, hillslope to basin cosmongenic nuclide concentration is examined in each sub-region to provide insight into the relative importance of erosion and transport on cosmogenic nuclide concentrations at each site. From this, important inferences about dominant geomorphic processes and the interpretation of cosmogenic nuclides can be made.

The Western Coastal Cordillera

Sampling efforts in the western Coastal Cordillera focused on sediments from the costal plain and alluvial fans that have apexes at the escarpment. The primary feature of this data set is a systematic increase in cosmogenic nuclide concentrations down the coastal plain. We suggest that this increase in cosmogenic nuclide concentrations reflects sediment transport time, a situation similar to that observed in the Mojave Desert (Nichols and others, 2002; Nichols and others, 2006). Sediment is deposited at the base of the coastal escarpment with a ^{10}Be concentration of $\sim 0.06 \times 10^6$ atoms g^{-1} (fig. 5D); this concentration is measured in three samples from fan apices and is equivalent to a simple exposure time of ~1,000 years or an erosion rate of ~100m/Ma (fig. 5D). As this sediment travels down and across the coastal plain towards the ocean, it acquires additional cosmogenic nuclides. Sediment samples collected further down the coastal plain have ^{10}Be concentration $>0.04 \times 10^6$ atoms g^{-1}, corresponding to exposure ages of >100 ka (fig. 5D). From this, it is inferred that samples spend a minimum of 100 ka in transport across the coastal plain. This estimate is a minimum, as production rates are reduced by an unknown amount due to cosmogenic nuclide attenuation in the active transport layer. A comparison of ^{10}Be concentrations from coarse and fine-grained sediment taken from some location in the Coastal Cordillera reveals that larger sediment has a higher ^{10}Be concentration and longer inferred travel time than finer-grained sediment; this situation is consistent with acquisition of significant cosmogenic nuclides during transport.

An erosion rate of ~ 100 m/Ma is inferred for the escarpment from cosmogenic nuclide concentrations in sediment at the apex of the alluvial fans. Erosion rates inferred from cosmogenic nuclides are broadly considered maximum erosion rates (for example, Lal and others, 1991), but in this situation additional cosmogenic nuclides are acquired since leaving the escarpment. These additional cosmogenic nuclides results in apparent erosion rates that are lower than actual escarpment erosion rate because it includes a substantial fan area with little to no erosion. These escarpment sediments are derived within the zone impacted by coastal fog (<1000 m); samples of bedrock above this elevation have ^{10}Be concentrations greater than 0.8×10^6 atoms g^{-1} (fig. 6), corresponding to erosion rates <4 m/Ma.

Interior Coastal Cordillera

The concentrations of cosmogenic nuclides inland of the escarpment increase in all types of sediment with increasing distance from the Pacific Ocean (fig. 6). This trend of higher cosmogenic nuclide concentration with decreasing precipitation is consistent with the observation that cosmogenic nuclide concentrations decrease within the escarpment at elevations above the fog zone. This trend is also consistent with the relationship described in Placzek and others (2010) and broadly consistent with the observation that the driest parts of the Atacama host rocks with some of the highest cosmogenic nuclide concentrations anywhere on Earth (Nishiizumi and others, 2005; Dunai and others, 2005; Kober and others, 2007; Evenstar and others, 2009; Amundson and others, 2012).

Detailed examination of cosmogenic nuclide concentrations from Site 1 provide further insight into the interpretation of cosmogenic nuclides in the eastern Coastal Cordillera. Two features of cosmogenic nuclide concentration at Site 1 require further examination: concentrations in sediment on the eastern side of the valley are much higher than concentrations in either the center or the western side of the valley and concentrations of cosmogenic nuclides in boulders is higher than that in sediment in the eastern side of the valley, but lower on the western side of the valley (fig. 7).

Cosmogenic nuclide concentrations in boulders from the western side of the valley are best explained by episodic exposure coupled with gradual transport down

the surface of the alluvial fan. The lower concentrations of cosmogenic nuclides in boulders relative to sediment suggests sudden and episodic production of boulders. Following boulder generation, the boulders move down the surface of the alluvial fan acquiring additional cosmogenic nuclides during transport, and boulders near the top of the fan have ^{10}Be concentrations corresponding to an exposure age of 90 ka; a boulder from further down the fan has a ^{10}Be concentration corresponding to an exposure age of 170 ka, and the boulder even further downslope has a ^{10}Be concentration corresponding to an exposure age of 380 ka (fig. 7D). However, these exposure ages represent exposure time of the sampled side boulder minus inherited cosmogenic nuclide concentration. Because these relatively small (<0.4 m) boulders likely flipped in transit, a minimum transit time can be inferred due to attenuation of cosmogenic nuclides when the currently exposed side is facing downward. However, this data suggest that boulder transport is very slow, with boulders moving downwards about 25 meters in elevation or 300 meters in distance over >190 ka.

Cosmogenic nuclide concentrations in a large cobble from the eastern side of the valley is much higher than that in associated sediment, a situation that is best explained by slow hillslope erosion of sediment, but with larger clasts that essentially do not erode. Sediment at this location was collected mid-hillslope and is likely representative of hillslope erosion rates at this locality. This pattern of much higher cosmogenic nuclide concentration in cobbles and boulders is observed throughout the hyperarid regions of the Atacama and contrasts with that observed in the wetter sub-regions of the Atacama such as the western side of the valley.

Questions naturally arise about interpretation of sediment in the axial drainage at Site 1. The locality-normalized and absolute concentration of cosmogenic nuclides in sediment from the axial drainage is slightly higher than that of the sediment from the western side of the valley (fig. 7). This implies that very little sediment in the axial drainage is derived from the eastern side of the valley, as such sediment input will leverage ^{10}Be concentrations higher. The low sediment input from the east is consistent with hillslope erosion rates that are >3.5 times faster on the western side of the valley. Two factors should result in locality-normalized concentrations in the axial drainage that are different from that at the fan apexes. The first of these factors is sediment travel time, which will result in higher cosmogenic nuclide concentrations in the axial drainage in a situation similar to that observed on the coastal plain. The second factor is production scaling. Cosmogenic nuclide production rates are ~10 percent higher at the apex of the fans (~100 m elevation difference) than in the axial drainage, and if samples from the fan were transported yesterday to the axial drainage and locality-normalized, then the normalized concentration of the sediment in the axial drainage would be 10 percent higher than that at the fan apex. Since the locality-normalized concentrations of cosmogenic nuclides is similar to that expected from a proportional mixture of material from the fan apexes, we suggest that both transport time and scaling differences approximately cancel each other and that an *apparent erosion rate* can be inferred from sediment in the axial drainage; this apparent erosion rate is broadly similar to the erosion rate on the hillslopes.

Overall, the inferred hillslope erosion rates from the eastern and interior Coastal Cordillera range between 0.4 and 2.5 m/Ma. Hillslope erosion rates determined from bedrock are between 2.5 and 0.6 m/Ma. These hillslope erosion rates are consistent with the apparent erosion rates inferred from channel sediment (2.5-0.4 m/Ma).

The Absolute Desert

Key trends in concentrations of cosmogenic nuclides in the absolute desert include: 1) higher cosmogenic nuclide concentrations in boulders and bedrock; 2) concentrations in sediment and boulders that generally decreases downslope, with minimum values occurring mid-slope; and 3) sediments in drainages that flow across

the absolute desert have cosmogenic nuclide concentrations that are different than that of local hillslopes and lower in the coarse-grained sediment (>1mm) than the 0.25 to 0.5 mm size.

Broadly, cosmogenic nuclide concentrations in boulders and bedrock from the absolute desert are higher than those measured in hillslope sediments. A critical inference from this relationship is that erosion rates are slower in material with subaerial exposure, a situation also observed in the eastern Coastal Cordillera. An obvious, but significant, implication is that different elements in the landscape spend different amounts of time near the surface and that these cosmogenic nuclide concentrations broadly reflect differential erosion rates, not the whole scale age of the landscape.

Concentrations of cosmogenic nuclides in sediment and boulders generally decrease downslope, with minimum values occurring on the slopes. This trend is best interpreted as production of sediment and boulders mid-slope, followed by acquisition of additional cosmogenic nuclides during transport, a situation similar to that observed in the Coastal Cordillera. For boulders located in boulder fields the primary mechanism for this transport is seismic shaking (Quade and others, 2012). Sediment, however, is likely transported downslope during rare rainfall events, a situation evidenced by poorly developed, but present, rilling and drainage networks on hillslopes. From this we infer that cosmogenic nuclide concentrations in sediments are broadly representative of hillslope erosion rates; whereas cosmogenic nuclide concentrations in boulders are more reflective of exposure ages of the boulders themselves.

Questions naturally arise about the interpretation of cosmogenic nuclides in sediment from fluvial channels that cut across the absolute desert. This sediment has two possible sources: local hillslopes or upland regions, such as the Cordillera Domeyko. Cosmogenic nuclide concentrations on the flanks of the Cordillera Domeyko are lower than those on hillslopes in the absolute desert. Sediments in the fluvial channels at Site 4 have cosmogenic nuclide concentrations that are lower in the fluvial channel than in adjacent alluvial surfaces. This, coupled with plant debris from the Cordillera Domeyko in this channel, implies that this sediment must be sourced in the Cordillera Domeyko. Two different grain sizes of sediment were analyzed from the fluvial sediment at Site 4 and the finer grained material has higher cosmogenic nuclide concentrations. This contrasts with the expected relationship between sediment travel times and grain size (for example, Clapp and others, 2000; Clapp and others, 2001; Matmon and others, 2003). One explanation for this relationship is that the finer and coarser grained material are composed of different proportions of local and extralocal material, with mostly smaller grains and higher cosmogenic nuclide concentrations derived locally and large material transported during rare floods originating in the highlands. At Site 3, cosmogenic nuclide concentrations in fluvial sediments are marginally higher than that at the base of local hillslopes, but cosmogenic nuclide concentration in finer grained material suggest a similar interpretation to Site 4.

The concentration of cosmogenic nuclides in hillslope sediments and bedrock in the absolute desert correspond to erosion rates between 0.4 and 1.1 m/Ma. Besides boulders, the only material with cosmogenic nuclide concentrations higher than this comes from sediment on inactive surfaces (discussed subsequently). Hillslope erosion rates of 0.47 to 0.97 m/Ma can be inferred from the mid-slope sediment at Sites 3 and 4, these sediments have the lowest cosmogenic nuclide concentration in our hillslope transects. Apparent erosion rates of 0.24 to 0.97 m/Ma are inferred from sediment samples in active features originating within the absolute desert; these apparent erosion rates are marginally lower than hillslope erosion rates, indicative of minor additional cosmogenic nuclides acquired during transport, but consistent with bed-

rock erosion rates. Thus, overall erosion rates of 0.2 to 1.5 m/Ma are inferred for the absolute desert.

Two sample localities in this study (Sites 4 and 5) are from surfaces that are inactive and potentially representative of ancient processes in the Atacama Desert. Understanding the geomorphic setting and cosmogenic nuclide concentrations at these sites is critical to understanding exposure ages from geomorphic features inferred to reflect the age of the Atacama Desert.

Interpretation of cosmogenic concentrations from desert pavement on the alluvial surface at Site 4 is best interpreted as a minimum exposure age of 3 Ma. Interpretation of cosmogenic nuclide concentrations for desert pavements remains controversial. For example, Quade (2001) argued that desert pavements might not serve as good surface age indicators due to disruption of surfaces during vegetative expansions. However, reliable minimum surface ages are reported from the Paran Plains in Israel (Matmon and others, 2009) and rejuvenation of desert pavement due to either vegetative expansions or other processes that might disrupt the surface is not likely to occur in the Atacama due to the extreme hyperaridity. The concentration of ^{10}Be in the stable alluvial surface corresponds to an age of 3.4 Ma. An inheritance of $\sim 2 \times 10^6$ atoms/gram (corresponding to ^{10}Be concentrations from the flanks of the Cordillera Domeyko) yields an exposure age of ~3 Ma for this sample. However, even minor erosion can significantly alter ^{10}Be exposure ages in this range towards a younger age (compare differences in age in two samples from boulder BA-11) and we consider 3 Ma as an absolute minimum age for this surface.

Exposure ages >6 Ma are reported only from site 5. However, the concentration of cosmogenic nuclides in sediment at site 5 is consistent with, but marginally higher than that determined for all other sites in the absolute desert. The observation that boulders at this site do not have the same concentration as the sediment on which they rest suggests that this surface has a complex sediment transport history. This complex history is not limited to surface exposure and one boulder on this fan surface has a minimum burial age of ~0.75 Ma. Another boulder at this site has ^{10}Be concentrations that are oversaturated with respect to every scaling scheme. This situation could either indicate inappropriate scaling or that production rates are underestimated because significant cosmogenic nuclides have been acquired by the sample at higher elevations.

The Cerros de los Tetas

The Cerro de los Tetas are characterized by relatively uniform cosmogenic nuclide concentrations. These concentrations do not vary with elevation. Furthermore, all samples from the Cerro de los Tetas have cosmogenic nuclide concentrations that overlap those in active material in the nearby absolute desert. This suggests that, within the uncertainty of our determinations, erosion rates at the crest of the Cerros de los Tetas are not significantly different than at the base. Similarly, inferred erosion rates from the Cerros de los Tetas are not significantly different from inferred erosion rates in the absolute desert despite evidence of slightly higher precipitation; this suggest that variables other than precipitation may influence erosion rates in the Atacama Desert. Inferred erosion rates for the Cerros de los Tetas are between 0.38 and 1.13 m/Ma (fig. 9C).

The Cordillera Domeyko

Bedrock, sediment, and boulders from the crest of the Cordillera Domeyko have cosmogenic nuclide concentrations that are higher than those from sediments on the flanks of the Cordillera Domeyko. At the crest of the Cordillera Domeyko cosmogenic nuclide concentrations in bedrock, fluvial sediment, and alluvial sediment all have similar concentrations of cosmogenic nuclides, suggesting that these concentrations

represent hillslope erosion rates of ~0.5 m/Ma on the crest of the Cordillera Domeyko. On the flanks of the Cordillera Domeyko, only sediment is available for sampling and is interpreted as apparent erosion rates with important caveats previously noted for such interpretation. An apparent erosion rate of ~3 m/Ma on the flanks of the Cordillera Domeyko is considerably faster than erosion rates from the crest of the Cordillera Domeyko. This is unexpected as vegetation, indicative of higher rainfall, is only present near the crest of the Cordillera Domeyko and suggests that variables other than precipitation must be an influence on erosion rates in the Cordillera Domeyko. It is likely that the other key variable is slope; the crest of the Cordillera Domeyko is relatively flat, particularly in comparison to the western and eastern flanks (figs. 12 and 13).

The Salars and the Andean Flank

The normalized concentration of cosmogenic nuclides in sediments from the western Andean flank systematically increase down the Andean flank and towards the Atacama desert. On the Andean Flank all samples are sediment samples and represent apparent erosion rates. These apparent erosion rates (1.1-30 m/Ma) increase with increased precipitation, consistent with the observation that erosion and aridity are related in the Atacama Desert. Sediments at the foot of the Andes have normalized concentrations that overlap those from the Andean flank, consistent with a source of these sediments on the Andean flank. However, boulders on the edge of salars have lower concentrations of cosmogenic nuclides than associated sediment and in a situation similar to that observed in the eastern Coastal Cordillera, this suggests episodic production of boulders from channel sides.

Generalized Trends in Cosmogenic Nuclide Concentrations

Observations of hillslope to basin trends in cosmogenic nuclide concentrations across our transects allow critical observations of the general trends in cosmogenic nuclide concentrations in hyperarid environments (eastern Coastal Cordillera, Cordillera Domeyko, Cerros de los Tetas, and absolute desert) and arid environments (western Coastal Cordillera and Andean Flank). These trends contrast with those observed in mesic environments; mesic environments are characterized by uniform cosmogenic nuclide concentrations in sediments, marginally higher cosmogenic nuclide concentration in bedrock, and lower cosmogenic nuclide concentrations in boulders (fig. 16A).

The hyperarid regions of the Atacama have a unique pattern of cosmogenic nuclide concentrations in different types of material (fig. 16C). The lowest cosmogenic nuclide concentrations are found in hillslope sediments. Bedrock has an intermediate cosmogenic nuclide concentration, which is similar to the concentration of cosmogenic nuclides in the youngest boulders. The cosmogenic nuclide concentration in boulders increases downslope and may reach saturation. Because sediment has relatively high cosmogenic nuclide concentrations on the hillslope, major changes in cosmogenic nuclide concentrations was not observed as a result of distance from hillslope. Sediment in active channels in the absolute desert often originates from regions with greater precipitation, this may result in higher cosmogenic nuclide concentrations in coarse-grained (local) sediment.

The arid regions of the Atacama have a pattern of cosmogenic nuclide concentrations consistent with that observed in other arid regions of the world (fig. 16B). In particular, the concentration of cosmogenic nuclides in sediment increases with distance away from the hillslope from which it originates; this influence of travel time also results in higher cosmogenic nuclide concentrations in coarser grained sediment. Bedrock may also have marginally higher cosmogenic nuclide concentrations than sediments. Boulders in such environments are produced episodically; this rapid

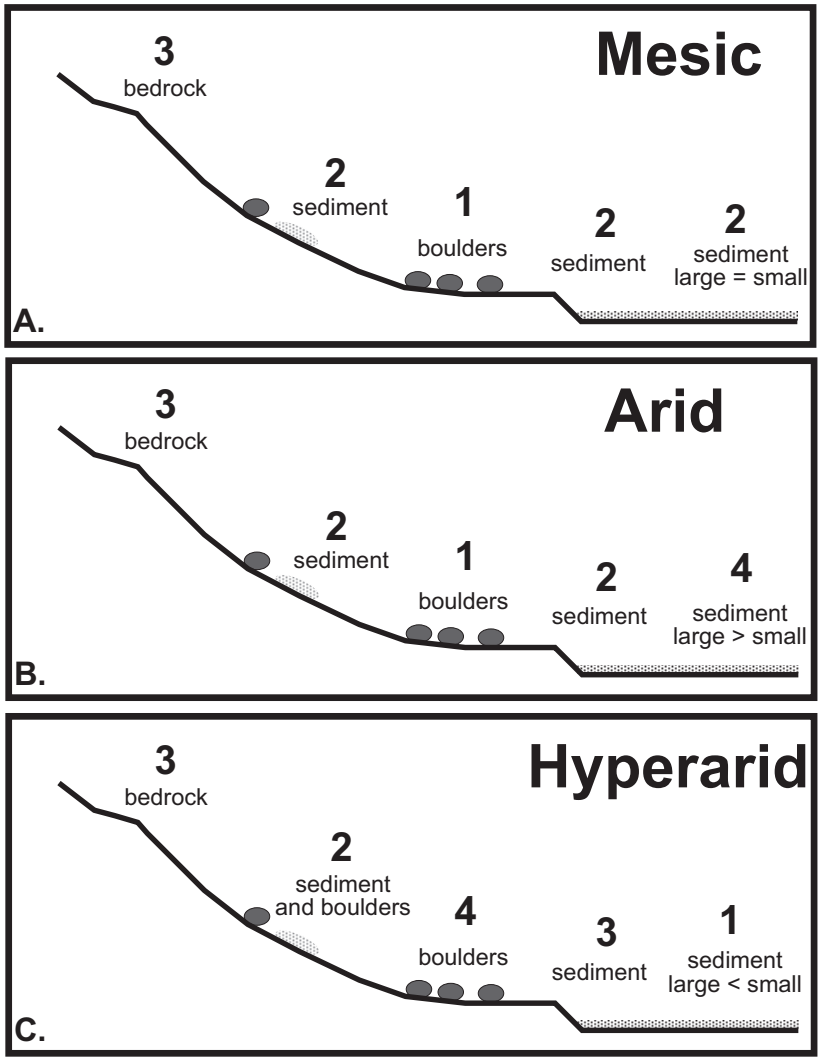

Fig. 16. Generalized relative concentration of cosmogenic nuclides in (A) mesic, (B) arid, and (C) hyperarid environments. Numbers represent relative concentrations of cosmogenic nuclides, with 0 representing the lowest and 4 the highest concentration.

boulder production results in generally lower concentrations of cosmogenic nuclides relative to sediments.

Comparison of Transects

In general, the northern and southern transects are broadly similar with respect to trends in cosmogenic nuclides. The highest concentrations of cosmogenic nuclides in both transects comes from erosion resistant boulders located directly east of the Coastal Cordillera. Cosmogenic nuclide concentrations in bedrock and sediment follow a similar trend in both transects; rapidly increasing inland from the coast reaching a maximum on the western flank of the Cordillera Domeyko and decreasing again towards the Andes. Along the AFZ, no discernable difference is observed

between erosion rates in the north and those towards the south (fig. 6). However, the location of the maximum concentration of cosmogenic nuclides is located farther east in the southern transect; similarly, a boulder with cosmogenic nuclide concentrations indicative of exposure ages >1.5 Ma is present east of the Cordillera Domeyko only in the southern transect. Moreover, a clear correlation between latitude and cosmogenic nuclide concentration is observed in the north-south transect along the salars (fig. 15A). We attribute the trend observed in figure 15B to greater precipitation in the north as a result of the increased influence of SASM.

Controls on Erosion Rates

The overall picture from both transects is that increased aridity greatly decreases hillslope and apparent erosion rates determined from sediments. The fastest erosion rates exceed 100 m/Ma and are located at the margins of the desert, the slowest apparent erosion rates are less than 0.1 m/My and occur in the absolute desert. In addition to the trend of increasing moisture towards both the east and the west, these transects contain two ranges that capture more precipitation than the surrounding lowlands, the Cerro de los Tetas and the Cordillera Domeyko; the broad relationship between precipitation and aridity is also observed for these ranges, but in detail results from the Cordillera Domeyko imply that an important secondary relationship between erosion rate and slope exists.

Precipitation across both transects ranges from negligible to 100 mm/yr and correlates with erosion rate (fig. 17A). This trend of higher apparent erosion rate with increasing precipitation is broadly consistent with the relationship described in Kober and others (2007); Placzek and others (2010) and Owen and others (2011). This relationship is also consistent with data from other global deserts (for example; Clapp and others, 2000; Bierman and Caffee, 2001; Bierman and Caffee, 2002; Abbuhi and others, 2010; Heimsath and others, 2010), suggesting that inferences from the central Atacama are broadly applicable to other deserts. This new data suggests that the relationship between aridity and erosion rates in the Atacama occurs over a range of precipitation, extending up to 100 mm/yr and extending well beyond the limit of hyperaridity (~10 mm/yr). Prior research in the Atacama suggests that the relationship between precipitation and erosion in the Atacama is a function of an erosion threshold that occurs at the boundary between vegetated and unvegetated desert (Owen and others, 2011). Here and in Carretier and others (2013) it is shown that in the Andes this relationship between erosion and aridity extents beyond the limit of the absolute desert and, for example, onto the vegetated zone of the Andean Flank (fig. 15A). This suggests that a simple threshold value below which low precipitation becomes relevant does not exist, instead precipitation becomes an increasingly important control on erosion as aridity increases. To place further constraints on the relationship between erosion rates and precipitation, we reexamined the data set in figure 2A, but only for regions with precipitation of 1000mm/yr or less (fig. 17B). This reexamination suggests that a relationship between erosion rate and precipitation extends across a much wider range of environments.

Precipitation is not the only influence on erosion rate in the central Atacama. The most notable exception to the correlation between aridity and erosion rate comes from the Cordillera Domeyko (figs. 13 and 14). The crest of the Cordillera Domeyko has an erosion rate that is slower than either the eastern or western flanks of this range. However, vegetation, indicative of higher rainfall, is only present near the crest of the Cordillera Domeyko. This suggests that differences in slope are large enough in this range to overcome the influence of greater precipitation at the crest.

At any given site, apparent erosion rates vary among different sample types. For example, the oldest boulders in the absolute desert essentially do not erode (erosion rates <0.1 m/Ma), but sediment is apparently being produced on hillslopes at rates

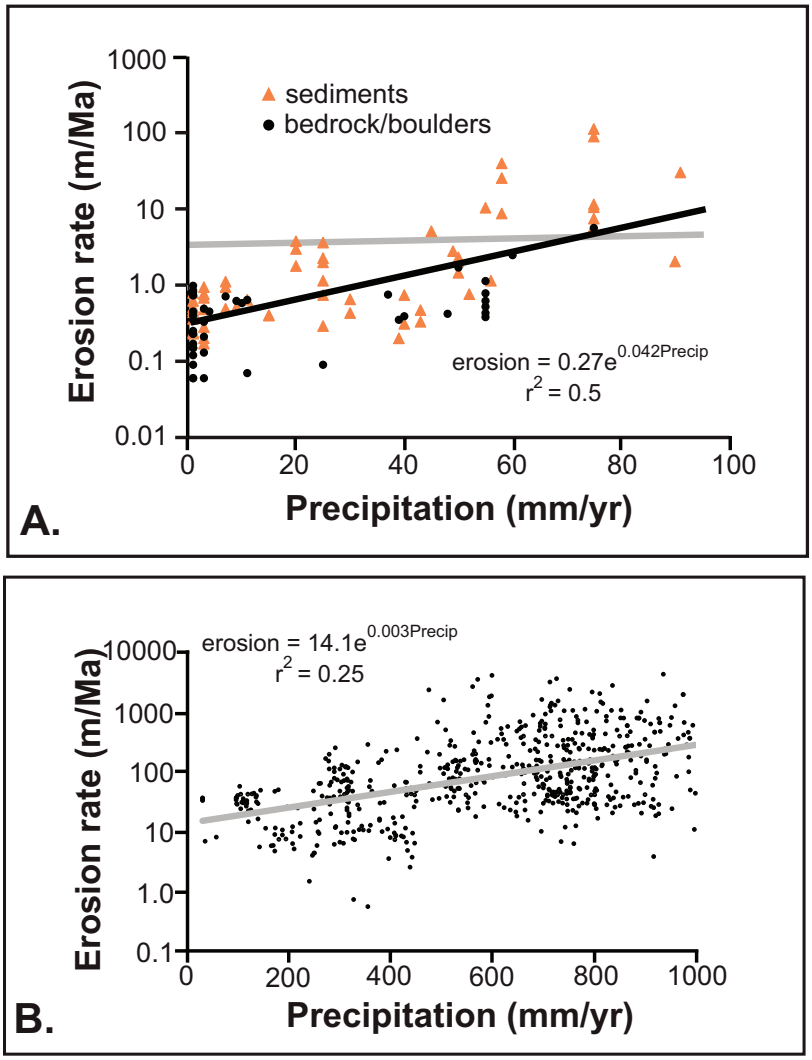

Fig. 17. (A) Erosion verses precipitation (log scale) in the central Atacama. Bedrock and boulder samples are represented as circles. Sediment samples are represented as triangles. (B) Apparent erosion verses precipitation over the range of zero to 1100 mm/yr. Data from Portenga and Bierman (2011).

approaching 1 m/Ma. It is likely that differential erosion rates develop at the same site because boulders and bedrock sit above the soil mantle. Rainfall rapidly runs off the exposed rock in this hyperarid environment, so bare rock is wetted for very short time periods despite millions of years of exposure. In that respect, the sensitivity of rocks in the Atacama to subaerial exposure is also an extension of the sensitivity of erosion rates in the Atacama to small changes in precipitation.

Erosion rates inferred for the coastal escarpment are the fastest observed in this study and are high by global standards. An erosion rate of ~100 m/Ma approaches uplift rates (100-250 m/Ma) estimated for the region (Ortlieb and others, 1996; Rech and others, 2006; fig. 18). A strong link between erosion rate and tectonic uplift is suggested by numerous studies in less extreme climates (Riebe and others, 2001a,

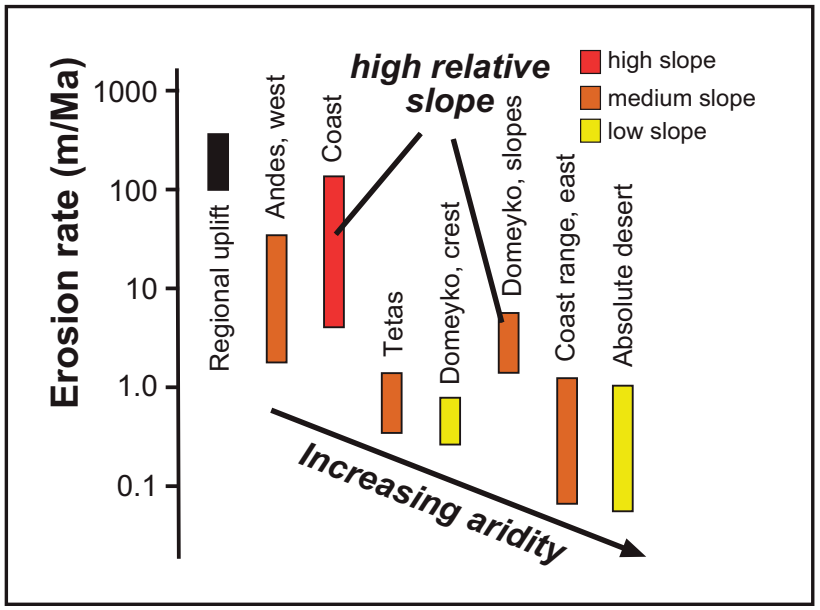

Fig. 18. Apparent erosion rates for various geomorphic sub-regions in the central Atacama. Regions are arranged from left to right in order of increasing aridity. In general, erosion rates decrease with decreasing precipitation; exceptions to this pattern result from the influence of slope, particularly the high slopes of the coastal escarpment and the low sloping crest of the Cordillera Domeyko. Erosion rate on the coastal escarpment are consistent with regional uplift rates (Ortlieb and others, 1996 and Rech and others, 2006).

2001b, 2003) and it is likely that given sufficient slope, precipitation, and hydrologic networks that connect hillslopes to base level, erosion rates in the central Atacama also approach uplift rates.

Implications for the Antiquity of the Atacama

Several aspects of our results suggest that the onset of hyperaridity in the Atacama Desert predates the Pliocene. First, a number of ages from boulders predate the Pliocene. Second, we offer new Miocene age constraints from a surface previously identified as Pliocene; the age of this surface previously formed a critical component in arguments for decreased incision rates in the late Pliocene. Third, we show that a site that is today very sensitive to sediment fluxes from modern storm events is at least 3 Ma in age. Finally, we show that most of the hillslopes in the central Atacama were exposed during the Quaternary and do not have complex exposure histories; this indicates the Atacama is not and probably never has been a frozen landscape.

In the central Atacama, the landscape consists of multiple elements that evolve at different rates. Most notably, we find that hillslopes are far more active features than low slope alluvial surfaces and that sediment moves downslope at a faster rate than boulders. Questions immediately arise as to if exposure ages from boulders and cobbles that are isolated from their point of origin represent the age of surface on which they rest and the age of the surrounding landscape as a whole; in this study these types of boulders are common at site 5. Questions about a potentially complex history of boulders is particularly pronounced for these boulders, as they may have a history that includes cosmogenic nuclides acquired at higher elevation and/or burial (for example, BA-6R1). These nuclides from higher elevation may potentially make significant contributions to stable (^{21}Ne, ^{3}He) cosmogenic nuclide measurements made by

Dunai and others (2005), Nishiizumi and others (2005), Kober and others, (2007), and Evenstar and others (2009). Broadly, however, exposure of boulders and cobbles for these long timescales (3-31 Ma) inherently implies lack of erosion in boulders, a process that is characteristic of hyperaridity (fig. 16B) even if it does not indicate that the individual surfaces are the age of the boulders.

Boulders in boulder fields can be clearly related to the bedrock from which they originate. Observations that these boulders are worn to smoothness in their midsections, often have a dished-out depression of sediments around the base, and have actually been observed to move past each other during a Mw 5.2 earthquake suggest that boulders within boulder fields are not moved by water, but rather by strong ground motion (Quade and others, 2012). The exposure age of these boulders also increases in age downslope and ranges between <1 Ma to saturated with respect to ^{10}Be (>~10 Ma). Sediment may move around these boulders at more rapid rates and under the influence of water. In many ways, the surface on which these boulders rest does not have a single age, but a composite age stretching from the Miocene (the oldest boulders) and into the Quaternary (the age of the sediment on the surface). However, the "age" of such surfaces has been used for estimates of ancient topography (Amundson and others, 2012). For such purposes, the "age" of the surface must be older than the age of the oldest boulder. Site 3 typifies a boulder field and is also the locality of maximum Miocene to Pliocene incision identified by Amundson and others, (2012) (fig. 10D). A Pliocene age is assigned to oldest surfaces at site 3 based on K-Ar ages from undescribed ash units (Amundson and others, 2012; fig. 10E). Here, we report boulder ages from the exact same region that are many millions of years old (>3 Ma) to saturated (~12 Ma) with respect to ^{10}Be. From this, it is clear that the topography at site 3 is Miocene in age; and this new surface "age" significantly reduces inferred Miocene to Pliocene incision rates for this site.

Rates of erosion and sediment export in the central Atacama are considerably more rapid for sediments than for boulders. The contrasting stability between sediment and boulders on surfaces in the Atacama Desert suggest that exposure ages for stable, but sediment covered, surfaces in the Atacama might place better age constraints on the most recent moisture pulses in the region. At Site 4, a stable desert pavement occurs on an alluvial surface and has a minimum age of 3 Ma. This site is located near the Atacama's eastern limit and drainage across this site is impacted by drainage from modern storms in the Cordillera Domeyko. Large scale stripping of the landscape in the Late Pliocene would likely cover the site by sediment, suggesting that the proposed event did not occur. Jordan and others (2014) suggest that the northern Atacama experienced marginally wetter intervals over the last 12 Ma. Wet intervals between 5.5 and 4.5 Ma and between 4 and 3.6 Ma are proposed by Jordan and others (2014) and might be correlative with the formation of this surface.

The cosmogenic nuclide exposure age implied by most material in the absolute desert is 0.7 to 1.5 Ma. Although bedrock and sediment samples are best interpreted as erosion rates, the exposure age of these samples gives important constraints on the timescale over which this sediment has resided at the surface. These ages suggest that the majority of hillslopes in the Atacama have been exposed in the Pleistocene. This is at odds with the suggestion by Amundson and others (2012) that widespread landscape evolution occurred in the Pliocene and was followed by the creation of a "frozen" Quaternary landscape.

CONCLUSIONS

Cosmogenic nuclides concentrations from the arid to hyperarid reaches of the central Atacama Desert were examined to quantify geomorphic processes in the central Atacama. Hillslope to basin changes in cosmogenic nuclide concentrations in each sub-region of the central Atacama suggest that these concentrations in bedrock

and sediment are best interpreted as erosion rates but also that apparent erosion rates from fluvial sediment is similar to hillslope erosion rate determined directly from hillslope sediments.

Erosion rates from the Atacama were examined to evaluate the dependence of erosion rates on environmental parameters. At a first order, this variability is most strongly tied to precipitation and this data set shows that the relationship between erosion and aridity extends beyond the limit of the absolute desert, suggesting that a simple threshold value below which low precipitation becomes relevant does not exist, but that instead precipitation becomes an increasingly important control on erosion as aridity increases. Here, it is suggested that this increase is gradual, extending perhaps to regions with precipitation as great as 1,000 mm/yr.

In detail, a number of other important observations illustrate the secondary, but strong, relationships between erosion rates and both subaerial exposure and slope across the central Atacama. At many locations in the absolute desert, boulders and bedrock have erosion rates lower than those inferred from fine-grained sediment at the same location; this suggests that boulders erode less rapidly than hillslope sediments because they sit above thick gypcrete soils. The relationship between erosion rates and slope is also strong, creating notable exceptions to the overarching trend of higher erosion rates in areas with higher precipitation. For example, despite higher precipitation in the Andes, apparent erosion rates from the steep coastal range are fast in comparison to apparent erosion rates from the Andean flank. Similarly, apparent erosion rates on the flanks of the Cordillera Domeyko are faster than rates at the flat crest. Taken together these patterns suggest that in the extreme environment of the Atacama, where bedrock erosion and sediment transport are limited by the scarcity of water, geomorphic rates are sensitive not only to changes in precipitation but also to variables such as slope, soil cover, and, potentially, uplift rate. The overall picture of landscape development in the central Atacama is, therefore, that aridity itself is very important in setting the rate of geomorphic process, but also that this aridity interacts with both slope and soil cover to influence erosion rates.

Understanding sediment production in the Atacama is essential to interpretation of cosmogenic nuclide ages as the timing of the onset of regional hyperaridity. Prior cosmogenic nuclide studies have focused primarily on remnant boulders to determine the ages of aridification; this new data set shows that these boulders do not have the same cosmogenic nuclide concentration as the surface on which they rest. Broadly, exposure of boulders and cobbles for million year timescales inherently implies lack of erosion over a long timeframe and indicates hyperaridity that is consistent with the exposure age of the boulders plus the prior exposure history of the boulder and minus erosion. Several lines of evidence suggest that the onset of hyperaridity in the Atacama Desert predates the Pliocene. For example, new Miocene exposure ages from boulders, including age constraints from a surface previously identified as Pliocene and forming a critical component in arguments for decreased incision rates in the late Pliocene are reported. Moreover, a site that is, today, very sensitive to sediment fluxes from modern storm events is at least 3 Ma in age. Moreover, most of the hilllslopes in the central Atacama were exposed during the Quaternary and do not have a complex exposure history—indicating that the Atacama remains an active, but slowly evolving landscape.

ACKNOWLEDGMENTS

Funding was provided by NSF01-01249 with additional field support from Chevron to the University of Arizona. We thank M. Caffee, A. Cyr, G. Michalski, P. Muzikar, and J. Rech for helpful discussions. We also thank A. Heimsath and anonymous reviewers.

References

Abbühl, L. M., Norton, K. P., Schlunegger, F., Kracht, O., Aldahan, A., and Possnert, G., 2010, El Niño forcing on ^{10}Be-based surface denudation rates in the northwestern Peruvian Andes: Geomorphology, v. 123, n. 3, p. 257–268, http://dx.doi.org/10.1016/j.geomorph.2010.07.017

Ahnert, F., 1970, Functional relationships between denudation, relief, and uplift in large, mid-latitude drainage basins: American Journal of Science, v. 268, n. 3, p. 243–263, http://dx.doi.org/10.2475/ajs.268.3.243

Alpers, C. N., and Brimhall, G. H., 1988, Middle Miocene climatic change in the Atacama Desert, northern Chile: Evidence from supergene mineralization at La Escondida: Geological Society of America Bulletin, v. 100, n. 10, p. 1640–1656, http://dx.doi.org/10.1130/0016-7606(1988)100<1640:MMCCIT>2.3.CO;2

Ammann, C., Jenny, B., Kammer, K., and Messerli, B., 2001, Late Quaternary glacier response to humidity changes in the Andes of Chile (18-29°S): Palaeogeography, Palaeoclimatology, Palaeoecology, v. 172, n. 3–4, p. 313–326, http://dx.doi.org/10.1016/S0031-0182(01)00306-6

Amundson, R., Dietrich, W., Bellugi, D., Ewing, S., Nishiizumi, K., Chong, G., Owen, J., Finkel, R., Heimsath, A., Stewart, B., and Caffee, M., 2012, Geomorphologic evidence for the late Pliocene onset of hyperaridity in the Atacama Desert: Geological Society of America Bulletin, v. 124, n. 7–8, p. 1048–1070, http://dx.doi.org/10.1130/B30445.1

Arancibia, G., Matthews, S. J., and Perez de Arce, C., 2006, K-Ar and ^{40}Ar/^{39}Ar Geochronology of supergene processes in the Atacama Desert, Northern Chile: tectonic and climatic relations: Journal of the Geological Society, v. 163, n. 1, p. 107–118, http://dx.doi.org/10.1144/0016-764904-161

Audin, L., Herail, G., Riquelme, R., Darrozes, J., Martinod, J., and Font, E., 2003, Geomorphological markers of faulting and neotectonic activity along the western Andean margin, northern Chile: Journal of Quaternary Science, v. 18, n. 8, p. 681–694, http://dx.doi.org/10.1002/jqs.787

Balco, G., and Rovey, C. W., II, 2008, An isochron method for cosmogenic-nuclide dating of buried soil and sediments: American Journal of Science, v. 308, n. 10, p. 1083–1114, http://dx.doi.org/10.2475/10.2008.02

Balco, G., Stone, J. O., Lifton, N. A., and Dunai, T. J., 2008, A complete and easily accessible means of calculating surface exposure ages or erosion rates from ^{10}Be and ^{26}Al measurements: Quaternary Geochronology, v. 3, n. 3, p. 174–195, http://dx.doi.org/10.1016/j.quageo.2007.12.001

Barnes, J. B., Ehlers, T. A., McQuarrie, N., O'Sullivan, P. B., and Pelletier, J. D., 2006, Eocene to recent variations in erosion across the central Andean fold-thrust belt, northern Bolivia: implications for plateau evolution: Earth and Planetary Science Letters, v. 248, p. 118–133, http://dx.doi.org/10.1016/j.epsl.2006.05.018

Betancourt, J. L., Latorre, C., Rech, J. A., Quade. J., and Rylander, K. A., 2000, A 22,000-year record of monsoonal precipitation from northern Chile's Atacama Desert: Science, v. 289, n. 5484, p. 1542–1546, http://dx.doi.org/10.1126/science.289.5484.1542

Bierman, P. R., and Caffee, M. W., 2001, Slow rates of rock surface erosion and sediment production across the Namib Desert and escarpment, Southern Africa: American Journal of Science, v. 301, n. 4–5, p. 326–358, http://dx.doi.org/10.2475/ajs.301.4-5.326

——— 2002, Cosmogenic exposure and erosion history of Australian bedrock landforms: Geological Society of America Bulletin, v. 114, n. 7, p. 787–803, http://dx.doi.org/10.1130/0016-7606(2002)114<0787:CEAEHO>2.0.CO;2

Carretier, S., Regard, V., Vassallo, R., Aguilar, G., Martinod, J., Riquelme, R., Pepin, E., Charrier, R., Hérrail, G., Farías, M., Guyot, J-L., Vargas, G., and Lagane, C., 2013, Slope and climate variability control of erosion in the Andes of central Chile: Geology, v. 41, n. 2, p. 195–198, http://dx.doi.org/10.1130/G33735.1

Chmeleff, J., von Blanckenburg, F., Kossert, K., and Jakob, D., 2010, Determination of the ^{10}Be- half-life by multicollector ICP-MS and liquid scintillation counting: Nuclear Instruments and Methods in Physics Research Section B-Beam Interactions with Materials and Atoms, v. 268, n. 2, p. 192–199, http://dx.doi.org/10.1016/j.nimb.2009.09.012

Clapp, E. M., Bierman, P. R., Schick, A. P., Lekach, J., Enzel, Y., and Caffee, M., 2000, Sediment yield exceeds sediment production in arid region drainage basins: Geology, v. 28, n. 11, p. 995–998, http://dx.doi.org/10.1130/0091-7613(2000)28<995:SYESPI>2.0.CO;2

Clapp, E. M., Bierman, P. R., Nichols, K. K., Pavich, M., and Caffee, M., 2001, Rates of sediment supply to arroyos from upland erosion determined using *in situ* produced cosmogenic ^{10}Be and ^{26}Al: Quaternary Research, v. 55, n. 2, p. 235–245, http://dx.doi.org/10.1006/qres.2000.2211

Clift, P. D., and Hartley, A. J., 2007, Slow rates of subduction erosion and coastal underplating: Geology, v. 35, n. 6, p. 503–506, http://dx.doi.org/10.1130/G23584A.1

Davis, M., Matmon, A., Placzek, C. J., McIntosh, W., Rood, D. H., and Quade, J., 2014, Cosmogenic nuclides in buried sediments from the hyperarid Atacama Desert, Chile: Quaternary Geochronology, v. 19, p. 117–126, http://dx.doi.org/10.1016/j.quageo.2013.06.006

Dillon, M. O., and Rundel, P. W., 1990, The botanical response of the Atacama and Peruvian desert floras to the 1982–83 El Niño event, *in* Glynn, P. W., editor, Global Ecological Consequences of the 1982–83 El Niño-Southern Oscillation: Amsterdam, Elsevier, North-Holland Press, p. 487–504.

Dunai, T. J., 2010, Cosmogenic Nuclides: Principles, Concepts and Applications in the Earth Surface Sciences: Cambridge, Cambridge University Press, Google eBook.

Dunai, T. J., Gonzáles López, G. A., and Juez-Larre, J., 2005, Oligocene-Miocene age of aridity in the Atacama Desert revealed by exposure dating of erosion-sensitive landforms: Geology, v. 33, n. 4, p. 321–324, http://dx.doi.org/10.1130/G21184.1

Evenstar, L. A., Hartley, A. J., Stuart, F. M., Mather, A. E., Rice, C. M., and Chong, G., 2009, Multiphase

development of the Atacama Planation Surface recorded by cosmogenic ^{3}He ages: Implications for uplift and Cenozoic climate change: Geology, v. 37, n. 1, p. 27–30, http://dx.doi.org/10.1130/G25437A.1

Ewing, S. A., Sutter, B., Owen, J., Nishiizumi, K., Sharp, W., Cliff, S. S., Perry, K., Dietrich, W., McKay, C. P., and Amundson, R., 2006, A threshold in soil formation at Earth's arid—hyperarid transition: Geochimica et Cosmochimica Acta, v. 70, n. 21, p. 5293–5322, http://dx.doi.org/10.1016/j.gca.2006.08.020

Fujioka, T., Chappell, J., Honda, M., Yatsevich, I., Fifield, K., and Fabel, D., 2005, Global cooling initiated stony deserts in central Australia 2–4 Ma, dated by cosmogenic ^{21}Ne-^{10}Be: Geology, v. 33, n. 12, p. 993–996, http://dx.doi.org/10.1130/G21746.1

Garzione, C. N., Molnar, P., Libarkin, J. C., and MacFadden, B. J., 2006, Rapid late Miocene rise of the Bolivian Altiplano: Evidence for removal of mantle lithosphere: Earth and Planetary Science Letters, v. 241, n. 3–4, p. 543–556, http://dx.doi.org/10.1016/j.epsl.2005.11.026

Gosse, J. C. and Phillips, F. M., 2001, Terrestrial *in situ* cosmogenic nuclides: theory and application: Quaternary Science Reviews, v. 20, n. 14, p. 1475–1560, http://dx.doi.org/10.1016/S0277-3791(00)00171-2

Granger, D. E., and Muzikar, P. F., 2001, Dating sediment burial with *in situ*-produced cosmogenic nuclides: theory, techniques, and limitations: Earth and Planetary Science Letters, v. 188, n. 1–2, p. 269–281, http://dx.doi.org/10.1016/S0012-821X(01)00309-0

Granger, D. E., Kirchner, J. W., and Finkel, R. C., 1997, Quaternary downcutting rate of the New River, Virginia, measured from differential decay of cosmogenic ^{26}Al and ^{10}Be in cave-deposited alluvium: Geology, v. 25, n. 2, p. 107–110, http://dx.doi.org/10.1130/0091-7613(1997)025<0107:QDROTN>2.3.CO;2

Granger, D. E., Lifton, N. A., and Willenbring, J. K., 2013, A cosmic trip: 25 years of cosmogenic nuclides in geology: Geological Society of America Bulletin, v. 125, n. 9–10, 1379–1402, http://dx.doi.org/10.1130/B30774.1

Gonzalez, G., Cembrano, J., Carrizo, D., Macci, A., and Schneider, H., 2003, The link between forearc tectonics and Pliocene-Quaternary deformation of the Coastal Cordillera, northern Chile: Journal of South American Earth Sciences, v 16, n. 5, p. 321–342, http://dx.doi.org/10.1016/S0895-9811(03)00100-7

Hartley, A. J., and Chong, G., 2002, Late Pliocene age for the Atacama Desert: Implications for the desertification of western South America: Geology, v. 30, n. 1, p. 43–46, http://dx.doi.org/10.1130/0091-7613(2002)030<0043:LPAFTA>2.0.CO;2

Heimsath, A. M., Chappell, J., and Fifield, K., 2010, Eroding Australia: rates and processes from Bega Valley to Arnhem Land, *in* Bishop, P., and Pillans, B., Australian Landscapes: Geological Society, London, Special Publications, v. 346, p. 225–241, http://dx.doi.org/10.1144/SP346.12

Hoke, G. D., Isacks, B.L, Jordan, T. E., and Yu, J. S., 2004, Groundwater-sapping origin for the giant quebradas of northern Chile: Geology, v. 32, n. 7, p. 605–608, http://dx.doi.org/10.1130/G20601.1

Houston, J., and Hartley, A. J., 2003, The central Andean west-slope rainshadow and its potential contribution to the origin of hyperarid in the Atacama Desert: International Journal of Climatology, v. 23, n. 12, p. 1453–1464, http://dx.doi.org/10.1002/joc.938

Jordan, T. E., Nester, P. L., Blanco, N., Hoke, G. D., Dávila, F., and Tomlinson, A. J., 2010, Uplift of the Altiplano-Puna plateau: A view from the west: Tectonics, v. 29, n. 5, TC5007, 33 p., http://dx.doi.org/10.1029/2010TC002661

Jordan, T. E., Kirk-Lawlor, N. E., Blanco, N., Rech, J. A., and Cosentino, N. J., 2014, Landscape modification in response to repeated onset of hyperarid paleoclimate states since 14 Ma, Atacama Desert, Chile: Geological Society of America Bulletin, B30978-1, http://dx.doi.org/10.1130/B30978.1

Jungers, M. C., Heimsath, A. M., Amundson, R., Balco, G., Shuster, D., and Chong, G., 2013, Active erosion–deposition cycles in the hyperarid Atacama Desert of Northern Chile: Earth and Planetary Science Letters, v. 371–372, p. 125–133, http://dx.doi.org/10.1016/j.epsl.2013.04.005

Klein, J., Giegengack, R., Middleton, P., Sharma, P., Underwood, J. R., Jr., and Weeks, R. A., 1986, Revealing histories of exposure using *in situ* produced ^{26}Al and ^{10}Be in Libyan desert glass: Radiocarbon, v. 28, n. 2A, p. 547–555.

Kober, F., Ivy-Ochs, S., Schlunegger, F., Baur, H., Kubik, P. W., and Wieler, R., 2007, Denudation rates and a topography-driven rainfall threshold in northern Chile: Multiple cosmogenic nuclide data and sediment yield budgets: Geomorphology, v. 83, n. 1–2, p. 97–120, http://dx.doi.org/10.1016/j.geomorph.2006.06.029

Kober, F., Ivy-Ochs, S., Zeilinger, G., Schlunegger, F., Kubik, P. W., Baur, H., and Wieler, R., 2009, Complex multiple cosmogenic nuclide concentration and histories in the arid Rio Lluta catchment, northern Chile: Earth Surface Processes and Landforms, v. 34, n. 3, p. 398–412, http://dx.doi.org/10.1002/esp.1748

Kohl, C. P., and Nishiizumi K., 1992, Chemical isolation of quartz for measurement of *in-situ*-produced cosmogenic nuclides: Geochimica et Cosmochimica Acta, v. 56, n. 9, p. 3583–3587, http://dx.doi.org/10.1016/0016-7037(92)90401-4

Korschinek, G., Bergmaier, A., Faestermann, T., Gerstmann, U. C., Knie, K., Rugel, G., Wallner, A., Dillmann, I., Dollinger, G., von Gostomski, C. L., Kossert, K., Maiti, M., Poutivtsev, M., and Remmert, A., 2010, A new value for the half-life of ^{10}Be by heavy-ion elastic recoil detection and liquid scintillation counting: Nuclear Instruments and Methods in Physics Research Section B-Beam Interactions with Materials and Atoms, v. 268, n. 2, p. 187–191, http://dx.doi.org/10.1016/j.nimb.2009.09.020

Lal, D., 1991, Cosmic ray labeling of erosion surfaces: *in situ* nuclide production rates and erosion models: Earth and Planetary Science Letters, v. 104, n. 2–4, p. 424–439, http://dx.doi.org/10.1016/0012-821X(91)90220-C

Langbein, W. B., and Schumm, S. A., 1958, Yield of sediment in relation to mean annual precipitation: Transactions, American Geophysical Union, v. 39, n. 6, p. 1076–1084.
Latorre, C., Betancourt, J. L., Rylander, K. A., and Quade, J., 2002, Vegetation invasions into Absolute Desert: A 45,000 yr rodent midden record from the Calama-Salar de Atacama Basins, northern Chile (lat 22°-24°S): Geological Society of America Bulletin, v. 114, n. 3, p. 349–366, http://dx.doi.org/10.1130/0016-7606(2002)114<0349:VIIADA>2.0.CO;2
Latorre, C., Betancourt, J. A., Rech, J. A., Quade, J., Holmgren, C., Placzek, C., Maldonado, A. J. C., Vuille, M., and Rylander, K. A., 2005, Late Quaternary history of the Atacama Desert, *in* Smith, M., and Hesse, P., editors, 23° S- Archaeology and Environmental History of the Southern Deserts: Canberra, Australia, National Museum of Australia Press, p. 73–90.
Lehmann, S. B., ms, 2013, Climatic and tectonic implications of a mid-Miocene landscape: examination of the Tarapaca Pediplain, Atacama Desert, Chile: Oxford, Ohio, Miami University, M S Thesis, 128 p.
Matmon, A., Bierman, P. R., Larsen, J., Southworth, S., Pavich, M., Finkel, R., and Caffee, M., 2003, Erosion of an ancient mountain range, the Great Smoky Mountains, North Carolina and Tennessee: American Journal of Science, v. 303, n. 9, p. 817–855, http://dx.doi.org/10.2475/ajs.303.9.817
Matmon, A., Simhai, O., Amit, R., Haviv, I., Porat, N., McDonald, E., Benedetti, L., and Finkel, R., 2009, Desert pavement-coated surfaces in extreme deserts present the longest-lived landforms on Earth: Geological Society of America Bulletin, v. 121, n. 5–6, p. 688–697, http://dx.doi.org/10.1130/B26422.1
Nichols, K. K., Bierman, P. R., Hooke, R. LeB., Clapp, E. M., and Caffee, M., 2002, Quantifying sediment transport on desert piedmonts using ^{10}Be and ^{26}Al: Geomorphology, v. 45, n. 1–2, p. 105–125, http://dx.doi.org/10.1016/S0169-555X(01)00192-1
Nichols, K. K., Bierman, P. R., Foniri, W. R., Gillespie, A. R., Caffee, M., and Finkel, R., 2006, Dates and rates of arid region geomorphic processes: GSA Today, v. 16, n. 8, p. 4–11, http://dx.doi.org/10.1130/GSAT01608.1
Nishiizumi, K., Caffee, M. W., Finkel, R. C., Brimhall, G., and Mote, T., 2005, Remnants of a fossil alluvial fan landscape of Miocene age in the Atacama Desert of northern Chile using cosmogenic nuclide exposure age dating: Earth and Planetary Science Letters, v. 237, n. 3–4, p. 499–507, http://dx.doi.org/10.1016/j.epsl.2005.05.032
Nishiizumi, K., Imamura, M., Caffee, M. W., Southon, J. R., Finkel, R. C., and McAninch, J., 2007, Absolute calibration of ^{10}Be AMS standards: Nuclear Instruments and Methods in Physics Research Section B: Beam Interactions with Materials and Atoms, v. 258, n. 2, p. 403–413, http://dx.doi.org/10.1016/j.nimb.2007.01.297
Ortlieb, L., Zazo, C., Goy, J. L., Hillaire-Marcel, C., Ghaleb, B., and Cournoyer, L., 1996, Coastal deformation and sea-level changes in the northern Chile subduction area (23°S) during the last 330 ky: Quaternary Science Reviews, v. 15, n. 8–9, p. 819–831, http://dx.doi.org/10.1016/S0277-3791(96)00066-2
Owen, J. J., Amundson, R., Dietrich, W. E., Nishiizumi, K., Sutter, B., and Chong, G., 2011, The sensitivity of hillsope bedrock erosion to precipitation: Earth Surface Processes and Landforms, v. 36, n. 1, p. 117–135, http://dx.doi.org/10.1002/esp.2083
Owen, J. J., Dietrich, W. E., Nishiizumi, K., Chong, G., and Amundson, R., 2013, Zebra stripes in the Atacama Desert: Fossil evidence of overland flow: Geomorphology, v. 182, p. 157–172, http://dx.doi.org/10.1016/j.geomorph.2012.11.006
Pananont, P., Mpodozis, C., Blanco, N., Jordan, T. E., and Brown, L. D., 2004, Cenozoic evolution of the northwestern Salar de Atacama Basin, northern Chile: Tectonics, v. 23, n. 6, TC6007, http://dx.doi.org/10.1029/2003TC001595
Portenga, E., and Bierman, P. R., 2011, Understanding Earth's Eroding Surface with ^{10}Be: GSA Today, v. 21, p. 4–10, http://dx.doi.org/10.1130/G111A.1
Placzek, C., Quade, J., Betancourt, J. L., Patchett, P. J., Rech, J. A., Latorre, C., Matmon, A., Holmgren, C., and English, N. B., 2009a, Climate in the dry, central Andes over geologic, millennial, and interannual timescales: Annals of the Missouri Botanical Garden, v. 96, p. 386–397, http://dx.doi.org/10.3417/2008019
Placzek, C., Quade, J., Rech, J. A., Patchett, P. J., and Pérez de Arce, C., 2009b, Geochemistry, chronology and stratigraphy of Neogene tuffs of the Central Andean region: Quaternary Geochronology, v. 4, n. 1, p. 22–36, http://dx.doi.org/10.1016/j.quageo.2008.06.002
Placzek, C. J., Matmon, A., Granger, D. E., Quade, J., and Niedermann, S., 2010, Evidence for active landscape evolution in the hyperarid Atacama measured from multiple terrestrial cosmogenic nuclides: Earth and Planetary Science Letters, v. 295, n. 1–2, p. 12–20, http://dx.doi.org/10.1016/j.epsl.2010.03.006
Placzek, C. J., Quade, J., and Patchett, P. J., 2013, A 130 ka record of rainfall on the Bolivian Altiplano: Earth and Planetary Science Letters, v. 363, p. 97–108, http://dx.doi.org/10.1016/j.epsl.2012.12.017
Quade, J., 2001, Desert pavements and associated rock varnish in the Mojave Desert: How old can they be?: Geology, v. 29, n. 9, p. 855–858, http://dx.doi.org/10.1130/0091-7613(2001)029<0855:DPAARV>2.0.CO;2
Quade, J., Reiners, P., Placzek, C., Matmon, A., Pepper, M., Ojha, K., and Murray, K., 2012, Seismicity and the strange rubbing boulders of the Atacama Desert, northern Chile: Geology, v. 40, n. 9, p. 851–854, http://dx.doi.org/10.1130/G33162.1
Rech, J. A., Quade, J., and Betancourt, J. L., 2002, Late Quaternary paleohydrology of the central Atacama Desert (lat 22°-24°S), Chile: Geological Society of America Bulletin, v. 114, n. 3, p. 334–348, http://dx.doi.org/10.1130/0016-7606(2002)114<0334:LQPOTC>2.0.CO;2
Rech, J. A., Currie, B. S., Michalski, G., and Cowan, A. M., 2006, Neogene climate change and uplift in the Atacama Desert, Chile: Geology, v. 34, n. 9, p. 761–764, http://dx.doi.org/10.1130/G22444.1
Riebe, C. S., Kirchener, J. W., Granger, D. E., and Finkel, R. C., 2001a, Strong tectonic and weak climatic

control of long-term chemical weathering rates: Geology, v. 29, n. 6, p. 511–514, http://dx.doi.org/10.1130/0091-7613(2001)029<0511:STAWCC>2.0.CO;2

——— 2001b, Minimal climatic control on erosion rates in the Sierra Nevada, California: Geology, v. 29, n. 5, p. 447–450, http://dx.doi.org/0.1130/0091-7613(2001)029<00447:MCCOER>2.0.CO;2

Riebe, C. S., Kirchner, J. W., and Finkel, C. R., 2003, Long-term rates of chemical weathering and physical erosion from cosmogenic nuclides and geochemical mass balance: Geochimica et Cosmochimica Acta, v. 67, n. 22, p. 4411–4427, http://dx.doi.org/10.1016/S0016-7037(03)00382-X

Scheuber, E., and Andriessen, P. A. M., 1990, The kinematic and geodynamic significance of the Atacama Fault zone, northern, Chile: Journal of Structural Geology, v. 12, n. 2, p. 243–257, http://dx.doi.org/10.1016/0191-8141(90)90008-M

Stone, J. O., 2000, Air pressure and cosmogenic isotope production: Journal of Geophysical Research-Solid Earth, v. 105, n. B10, p. 23753–23759, http://dx.doi.org/10.1029/2000JB900181

von Blanckenburg, F., 2006, The control mechanisms of erosion and weathering at basin scale from cosmogenic nuclides in river sediment: Earth and Planetary Science Letters, v. 242, n. 3–4, p. 224–239, http://dx.doi.org/10.1016/j.epsl.2005.11.017

von Blanckenburg, F., Belshaw, N. S., and O'Nions, R. K., 1996, Separation of ^{9}Be and cosmogenic^{10}Be from environmental materials and SIMS isotope dilution analysis: Chemical Geology, v. 129, n. 1–2, p. 93–99, http://dx.doi.org/10.1016/0009-2541(95)00157-3

Vuille, M., and Ammann, C., 1997, Regional snowfall patterns in the high, arid Andes: Climatic Change, v. 36, n. 3–4, p. 413–423, http://dx.doi.org/10.1023/A:1005330802974

Vuille, M., and Keimig, F., 2004, Interannual variability of summertime convective cloudiness and precipitation in the central Andes derived from ISCCP-B3 data: Journal of Climate, v. 17, n. 17, p. 3334–3348, http://dx.doi.org/10.1175/1520-0442(2004)017<3334:IVOSCC>2.0.CO;2

Willenbring, J. K., Codilean, A. T., and McElroy, B., 2013, Earth is (mostly) flat: Apportionment of the flux of continental sediment over millennial time scales: Geology, v. 41, n. 3, p. 343–346, http://dx.doi.org/10.1130/G33918.1

Zhou, J., and Lau, K.-M., 1998, Does a monsoon climate exist over South America?: Journal of Climate, v. 11, n. 5, p. 1020–1040, http://dx.doi.org/10.1175/1520-0442(1998)011<1020:DAMCEO>2.0.CO;2